Nucleic Acids Research, 2025, **53**, gkaf160
https://doi.org/10.1093/nar/gkaf160
RNA and RNA-protein complexes

RNA anchoring of Upf1 facilitates recruitment of Dcp2 in the NMD decapping complex

Nadia Ruiz-Gutierrez[1], Jeanne Dupas[1], Elvire Auquier[1], Irène Barbarin-Bocahu[2], Claudine Gaudon-Plesse[3], Cosmin Saveanu[4], Marc Graille[2], Hervé Le Hir[1,*]

[1]Institut de Biologie de l'Ecole Normale Supérieure (IBENS), Ecole normale supérieure, CNRS, INSERM, PSL Research University, 46 rue d'Ulm, 75005 Paris, France
[2]Laboratoire de Biologie Structurale de la Cellule (BIOC), CNRS, Ecole polytechnique, Institut Polytechnique de Paris, 91120 Palaiseau, France
[3]Institut de Génétique et de Biologie Moléculaire et Cellulaire (IGBMC), CNRS UMR 7104, INSERM, U1258, Université de Strasbourg, Illkirch, France
[4]Institut Pasteur, Université Paris Cité, Unité de Biologie des ARN des Pathogènes Fongiques, 75015 Paris, France
[*]To whom correspondence should be addressed. Email: herve.lehir@bio.ens.psl.eu

Abstract

Upf1 RNA helicase is a pivotal factor in the conserved nonsense-mediated mRNA decay (NMD) process. Upf1 is responsible for coordinating the recognition of premature termination codons (PTCs) in a translation-dependent manner and subsequently triggering mRNA degradation. Multiple factors assist Upf1 during these two consecutive steps. In *Saccharomyces cerevisiae*, Upf2 and Upf3 associated with Upf1 (Upf1-2/3) contribute to PTC recognition but are absent from the Upf1-decapping complex that includes Nmd4, Ebs1, Dcp1, and Dcp2. Despite their importance for NMD, the organization and dynamics of these Upf1-containing complexes remain unclear. Using recombinant proteins, here we show how distinct domains of Upf1 make direct contacts with Dcp1/Dcp2, Nmd4, and Ebs1. These proteins also bind to each other, forming an extended network of interactions within the Upf1-decapping complex. Dcp2 and Upf2 compete for the same binding site on the N-terminal CH domain of Upf1, which explains the presence of two mutually exclusive Upf1-containing complexes in cells. Our data demonstrate that Nmd4-assisted recruitment of Upf1 promotes anchoring of the decapping enzyme to NMD targets.

Graphical abstract

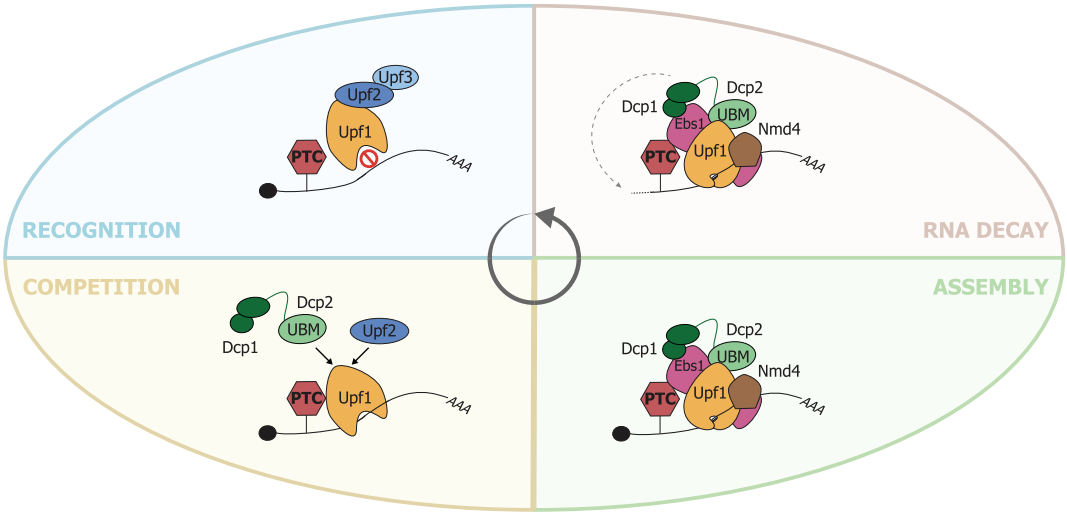

Introduction

To ensure correct cellular function, transcriptome homeostasis and attenuation of deleterious effects of gene expression errors, multiple quality control pathways quickly degrade aberrant transcripts. Nonsense-mediated mRNA decay (NMD) is a conserved translation-dependent messenger RNA degradation pathway that recognizes and degrades mRNAs bearing premature termination codons (PTCs) as well as many

Received: October 29, 2024. **Revised:** February 6, 2025. **Editorial Decision:** February 14, 2025. **Accepted:** February 18, 2025

physiological transcripts lacking PTCs [1–4]. Hence, NMD is implicated in a wide range of cellular processes, including differentiation [5, 6], stress response [7], and immune surveillance [8, 9]. Thus, NMD deregulation is linked to several pathologies, including cancer [10], neurodegeneration [11], and genetic disorders [12].

NMD likely unfolds in two sequential stages: an initial recognition of RNA targets followed by the recruitment of decay factors that irreversibly trigger RNA degradation. These coordinated and successive steps are governed by the evolutionarily conserved RNA helicase Upf1 [13, 14]. Upf1 binds nucleic acids (NAs) and is able to translocate directionally along RNA using the energy from ATP hydrolysis [15–17]. Thus, it can unwind double-stranded NA, translocate along single-stranded NA, and remodel mRNPs *in vitro* [15, 16, 18]. Its helicase activity, ATPase activity, and processivity are essential for efficient target recognition and degradation *in vivo* [17, 19]. Together with Upf2 and Upf3, the Upf proteins form a trimeric complex (Upf1-2/3) essential for NMD [20, 21]. However, the precise sequence of events, from Upf1 recruitment to the onset of degradation, is not completely understood.

In the yeast *Saccharomyces cerevisiae* (*S.c.*), NMD is triggered by a PTC distant from the poly (A) tail [22]. An increased distance between the terminating ribosome and the poly (A) binding proteins decreases the efficiency of translation termination [23, 24]. Consequently, it likely provides time for the Upf1-2/3 trimeric complex to be recruited onto the target mRNA. In mammals and other metazoans, additional layers of regulation contribute to the complexity of NMD [25]. These include Upf1 phosphorylation [26, 27] and interactions with specific partners, such as Smg1, Smg6, and Smg5/7 [28–30]. The presence of a stop codon at least 50–55 nucleotides upstream a spliced junction carrying an exon junction complex also elicits NMD [31–33].

Degradation of metazoan NMD targets can be achieved by different RNA-decay mechanisms including decapping [34, 35], endonucleolytic cleavage [36–38], and deadenylation [39, 40]. In yeast, the degradation of NMD targets is mostly attributed to deadenylation-independent decapping [41]. The decapping process relies on the catalytic activity of Dcp2, assisted by its essential cofactor Dcp1 [42, 43]. This heterodimeric complex hydrolyses the 5′ cap structure leading to a 5′ phosphorylated RNA fragment that is tailored for subsequent degradation by the processive exonuclease Xrn1 [44]. Regardless of the organism, initiation of RNA decay, often through decapping, is a key step that significantly influences the degradation process. Thus, triggering of decapping must be precise and stringently regulated to avoid off-target degradation. Therefore, decapping activity is regulated by an array of additional cofactors conferring target specificity [42, 43].

Previous quantitative mass spectrometry analyses of NMD complexes in *S.c.* revealed the existence of two distinct and mutually exclusive Upf1-bound complexes: the conserved Upf1-2/3 core complex and the Upf1-decapping complex that includes the heterodimer Dcp1/Dcp2 and its cofactor Edc3, as well as the NMD cofactors Nmd4 and Ebs1, and the protein kinase Hrr25 [45]. Analyses of these complexes in strains lacking Upf2 or Nmd4 show their sequential assembly, with the Upf1-2/3 complex forming prior to the NMD decapping complex [45]. The existence of two distinct Upf1-bound complexes suggests direct regulation of RNA degradation by Upf1-mediated recruitment of decay-inducing partners. Interactions between Upf1 and Dcp2 have been previously established by two-hybrid experiments and coimmunoprecipitation studies in yeast and humans [40, 46, 47]. However, understanding Upf1 recruitment mechanisms, as well as the intricate chronology of Upf1-bound complexes, is constrained by the inherent dynamism and transient nature of these complexes. As a result, the mechanisms governing the recruitment and the dynamic interplay of components in NMD complexes remain elusive.

Here, we investigate the molecular bases of the formation and function of the Upf1-2/3 and Upf1-decapping complexes in yeast by dissecting direct protein–protein interactions *in vitro* using recombinant proteins. We demonstrate that Upf1 directly interacts with Ebs1, Nmd4, and the decapping heterodimer Dcp1/Dcp2. The two Upf1-binding motifs (UBMs) of Dcp2 compete with Upf2 for interaction with Upf1. Furthermore, we show that Upf1 is anchored to the mRNA in the presence of Dcp2 and Nmd4, contrary to the Upf1–Upf2 complex. Altogether, our thorough biochemical characterization provides new insights into the successive events leading to mRNA degradation during NMD.

Materials and methods

cDNA cloning

S.c. Upf1 full-length (FL, pHL1280), helicase domain (HD, pHL1281), and CH-HD truncation (pHL 1282) (Uniprot accession code: P30771) were cloned into a homemade variant of pET28a vector (Novagen) containing calmodulin-binding protein (CBP) coding sequence (pHL5) and hexa-histidine tag (6-His or His) coding sequence. Polymerase chain reaction (PCR) products were amplified using HLH2703/HLH2704, HLH2705/HLH2706, and HLH2707/HLH2706, respectively, and were inserted between NheI/XhoI. Truncations (CH, HD-Ct, and Ct, respectively pHL1603, pHL1559, and pHL1566) were cloned by PCR amplification using phosphorylated oligonucleotides followed by ligation using HLH3765/HLH2824, HLH3641/HLH3642, and HLH3641/HLH3643 as oligonucleotides respectively and pHL1280 as matrix. Domain boundaries were defined according to previous studies [16].

S.c. Dcp2-UBM (pHL1637) (Uniprot accession code: P53550) was amplified using HLH3826/HLH3841 and cloned into pGEX-6P-1 vector (Cytiva) between BamHI/NotI. *S.c.* Dcp2-UBM1 (aa 434–508, pMG621) and UBM2 (aa 690–720, pMG676) were also cloned into pGEX-6P-1 vector between BamHI/NotI. GST-Dcp1 (pBS4576) and GST-Dcp1/Dcp2-S aa 1–315, pBS5135) were generated as described in [48]. Dcp2-L2 (aa 1–663) and Dcp2-L (aa 1–720) were cloned into pBS5135. For *S.c.* Dcp2-UBM-4R mutant (pHL 1937), a gene block containing the modified sequence was ordered from Eurofins and cloned into pGEX-6P-1 vector between BamHI/NotI.

S.c. Nmd4 full-length coding sequence (Uniprot accession code: Q12129) was provided by C. Saveanu [45]. The sequence was cloned into a homemade variant of pET28a vector (Novagen) containing Twin-Strep-tag (TS) coding sequence (pHL1567) to produce TS-Nmd4-His. It was cloned into pHL5 to produce CBP-Nmd4-His. To produce the C-terminal His-tagged version, it was cloned into pet28a. Finally, the pMG838 plasmid expressing the HisZZ-tagged Nmd4 protein was generated as described in [49].

S.c. Ebs1 (1–591) coding sequence (Uniprot accession code: Q03466) was provided by C. Saveanu [45] and cloned into a homemade variant of pET28a (Novagen) containing Glutathion-S-Transferase coding sequence (pHL6) to obtain pHL1513 or CBP (pHL5) to obtain pHL1514. Both PCR products were amplified using Ebsrev/Ebsfw and inserted between NdeI and XhoI. To produce the His-SUMO-tagged version, Ebs1 (1–591) was amplified using HLH3801/HLH3802 and inserted between NotI and XhoI into a modified pBR322 vector with His-SUMO tag at the 3′ end [50].

S.c. Upf2 (933–1089) coding sequence (Uniprot accession code: P38798) was amplified using Upf2-933-NdeI-for/Upf2-1089-NotI-rev and cloned between NdeI/NotI into a modified pET9b vector with an addition of a sequence coding for an hexahistine tag at the 3′ end of the gene (pMG462).

The CBP-HisZZ plasmid was cloned by Gibson assembly using a gene block containing CBP coding sequence ordered from IDT inserted between NcoI and NdeI within a pet28b vector containing the HisZZ coding sequence [49].

Oligonucleotides:

HLH2703 (ctagacgctagcatggtcggttccggttctcacac)

HLH2704 (catgacctcgagtattcccaaattgctgaagtcttttgac)

HLH2705 (ctagacgctagcgaacaggaagcaatcccacc)

HLH2706 (catgacctcgagaggacgaactaattgaacagtgc)

HLH2707 (ctagacgctagctcgccttcagcttcagac)

HLH3765 (ctctggggcgtcaatatcattaatt)

HLH2824 (ctcgagcaccaccaccacc)

HLH3641 (gctagccatatgctccttatcg)

HLH3642 (gaacaggaagcaatcccacc)

HLH3643 (cagccaagaaagactgaacg)

HLH3826 (cctgggatccagcagctcctcccctgg)

HLH3841 (cgatgcggccgcaagctttttttatcattcgccagac)

Upf2-933-NdeI-for (gggaacatatgagcgactctgatttggagtatggtg g)

Upf2-1089-NotI-rev (gggaacatatgcaccatcaccatcaccatgttcgaaagaacgttttaaaacaat ctttttaatcttgtttcgc)

Ebsfw (cccatatggctagcatggaaccatcga)

Ebsrev (gtggtgctcgagcttaaatccaa)

HLH3801 (aaaccggcggccgcatggaaccatcgaatacccaaaaag)

HLH3802 (tcacgttatatctttaataagaaaattggatttaagtgactcgagc accac)

Protein overexpression and purification

BL21 (DE3)-CodonPlus competent *Escherichia coli* bacteria (Agilent) were transformed with 500 ng of plasmid of interest by 2 min at 42°C heat shock. After addition of 1 ml of liquid Lysogeny Broth (LB) media and 1-h incubation at 37°C, cells were pelleted by 4 min centrifugation at 3500 *g*. The pellet was resuspended in 50 µl of LB media, plated in antibiotic containing LB plates, and left to grow overnight at 37°C. 2–3 colonies were resuspended in 25 ml of LB liquid media containing antibiotic in a 250 ml of Erlenmeyer flask and incubated at 37°C, 200 rpm for 4 h. The bacteria were inoculated in 1 l of autoinducible LB or TB (Terrific Broth) containing metals (Formedium) added with the plasmid antibiotic resistance (ampicillin 100 µg/ml or kanamycine 50 µg/ml) and chloramphenicol (25 µg/ml) in a 5-l Erlenmeyer flask and incubated at 18°C, 200 rpm overnight. Bacterial cultures were pelleted by 10 min, 4000 *g* centrifugation at 4°C. The pellet was resuspended in 25 ml of His-Lysis Buffer [1.59 mM KH_2PO_4, 4.5 mM, Na_2HPO_4, 231 mM NaCl, 1 mM MgAc2, 0.1% NP-40, 20 mM imidazole, 10% (v/v) glycerol, 2 mM Dithiothreitol (DTT), pH 7.0]. Before sonication, 1× of protease inhibitors (Apoprotinine, Leupeptine, PMSF, Pepstatin) were added. Samples were sonicated in a metal beaker at 30% amplitude and 1-s pulse during 4 min. To keep low temperatures, the beaker was placed on a mix of dry ice and ice. The bacterial debris were pelleted by centrifugation for 30 min at 18 000 rpm. The supernatant was retrieved and mixed with 1 ml of Nickel-NTA Agarose slurry (Qiagen) equilibrated with His-Lysis Buffer. The sample was incubated in a rotator for 1 h at 4°C before centrifugation at 4000 rpm for 5 min at 4°C to pellet the beads. The supernatant was removed, and the beads were washed with 25 ml of His-Lysis Buffer. The beads were transfered into a Poly-Prep chromatography column (Bio-Rad) pre-equilibrated with 1 ml of lysis buffer. The column was washed with 5 ml of His-lysis buffer then with 5 ml of His-wash buffer [1.59 mM KH_2PO_4, 4.5 mM, Na_2HPO_4, 231 mM NaCl, 250 mM NaCl, 1 mM $MgAc_2$, 0.1% NP-40, 50 mM imidazole, 10% (v/v) glycerol, 2 mM DTT, pH 7.0], then again with 5 ml of His-lysis buffer. The column was closed and the resin was incubated with 1 ml of His-elution buffer [1.59 mM KH_2PO_4, 4.5 mM, Na_2HPO_4, 231 mM NaCl, 1 mM $MgAc_2$, 0.1% NP-40, 250 mM imidazole, 10% (v/v) glycerol, 2 mM DTT, pH 7.0] for 10 min at 4°C. Elution was performed successively with 1 ml of elution buffer, and protein concentrations were measured by Bradford Assay. The fractions with highest concentration were pooled together and dialysed overnight. For CBP-tagged proteins, dialysis was performed against 1 l of Calmodulin Binding Buffer (CBB) [10 mM Tris–HCl, pH 7.5, 250 mM NaCl, 1 mM $MgAc_2$, 4 mM $CaCl_2$, 0.05% NP-40, 10% (v/v) glycerol, and 2 mM DTT] at 4°C. The dialysed fractions were retrieved and mixed with 500 µl of Calmodulin Sepharose 4B resin (50% Slurry, GE Healthcare) washed with CBB. The samples were incubated in a rotor for 2 h at 4°C, and then transferred into a Poly-Prep chromatography column (Bio-Rad) pre-equilibrated with 1 ml of CBB. After one wash with 5 ml of CBB the column was closed and the resin was incubated with 500 µl of Calmodulin Elution Buffer [10 mM Tris–HCl, pH 7.5, 250 mM NaCl, 1 mM $MgAc_2$, 0.05% NP-40, 20 mM EGTA, 10% (v/v) glycerol, and 2 mM DTT] for 10 min at 4°C. Elution was performed successively with 500 µl of Calmodulin Elution Buffer, and protein concentrations were measured by Bradford Assay. For GST- and TS-tagged proteins, purification steps were similar but performed using different buffers. For GST-tagged proteins, dialysis or lysis was performed against GST-Binding Buffer [20 mM Tris–HCl, pH 8.0, 200 mM NaCl, 5 mM β-mercaptoethanol, and 1 mM $MgCl_2$], the resin used was Glutathione Sepharose 4B (GE Healthcare), and proteins were eluted with GST Elution Buffer [50 mM Tris–HCl, pH 7.5, 250 mM KCl, 1 mM MgAc2, 1 mM DTT, 0.005% NP-40, 10% (v/v) glycerol, and 10 mM L-glutathione reduced]. For TS-tagged proteins, dialysis was performed against TS-binding buffer [10 mM Tris–HCl, pH 8, 150 mM NaCl, 0.1% NP-40, and 1 mM DTT]. Strep-Tactin resin (Iba) was used for protein binding, and proteins were eluted with TS elution buffer (10 mM Tris–HCl, pH 8, 150 mM NaCl, 0.1% NP-40, 1 mM DTT, and 2.5 mM D-Desthiobiotin). For all eluted proteins, the highest concentrated fractions were pooled together and dialysed overnight against 1 l of storage buffer [1.59 mM KH_2PO_4, 4.5 mM, Na_2HPO_4, 231 mM NaCl, 1 mM MgAc2, 10% (v/v) glycerol, and 2 mM DTT, pH 7.0]. The dialysed proteins were aliquoted

in small volumes depending on the final protein concentration and stored at −80°C [51, 52].

The *S.c.* Upf2 (933–1089)-His protein was over-expressed from pMG462 in *E. coli* BL21 (DE3) CodonPlus cells in 1 l of TBAI containing kanamycin (100 μg/ml) and chloramphenicol (25 μg/ml). After a 3 h incubation at 37°C, the bacteria were incubated overnight at 18°C. Cells were harvested by centrifugation at 4000 rcf for 30 min at 4°C, resuspended in buffer Lysis Buffer B (20 mM Tris–HCl pH 8.0, 200 mM NaCl, and 5 mM β-mercaptoethanol), and lysed by sonication after addition of 200 μl of phenylmethylsulfonyl fluoride (PMSF, 100 mM). The protein was first purified on a Protino® Ni-NTA agarose resin pre-equilibrated with buffer Lysis Buffer B. After successive washing steps using first Lysis buffer B and then high-salt buffer (20 mM Tris–HCl, pH 8.0, 1 M NaCl, and 5 mM β-mercaptoethanol), the proteins were eluted using Lysis buffer B supplemented with 400 mM imidazole pH 7. The eluted protein was loaded on a HiTrap Heparin (Cytiva) column pre-equilibrated in buffer A_{50} and eluted using a linear gradient from 100% of low-salt buffer (20 mM Tris–HCl, pH 8.0, 50 mM NaCl, and 5 mM β-mercaptoethanol) to 100% of high-salt buffer. Finally, the protein was purified on a S75-16/60 size-exclusion column (Cytiva) equilibrated with Lysis buffer B supplemented with 10% (v/v) glycerol.

The HisZZ-tagged Nmd4 protein was purified as described in [49].

The CBP-His-ZZ protein was over-expressed from pHL1662 in *E. coli* BL21 (DE3) Gold cells in 1 l of TBAI containing kanamycin (100 μg/ml). After a 3 h incubation at 37°C, the bacteria were incubated overnight at 25°C. Cells were harvested by centrifugation at 4000 rcf for 30 min at 4°C, resuspended in buffer Lysis Buffer C (20 mM Tris–HCl, pH 7.5, 200 mM NaCl) and lysed by sonication after addition of 200 μl of PMSF (100 mM). The protein was first purified on a Protino® Ni-NTA agarose resin pre-equilibrated with buffer Lysis Buffer C. After successive washing steps using first Lysis buffer C and then high-salt buffer (20 mM Tris–HCl pH 7.5, 1 M NaCl), the proteins were eluted using Lysis buffer C supplemented with 250 mM imidazole pH 7. The eluted protein was loaded on a HiTrap Q (Cytiva) column pre-equilibrated in Lysis buffer C and eluted using a linear gradient from 100% of Lysis buffer C to 100% of high-salt buffer. Finally, the protein was purified on a S75-16/60 size-exclusion column (Cytiva) equilibrated with Lysis buffer C.

Protein and RNA pulldown assays

Six micrograms of each protein of interest were mixed in a Protein LoBind tube (Eppendorf) and volume was completed to 30 μl with Storage Buffer [1.59 mM KH_2PO_4, 4.5 mM, Na_2HPO_4, 231 mM NaCl, 1 mM MgAc2, 10% (v/v) glycerol, and 2 mM DTT, pH 7.0]. A 5 μl of sample was retrieved from each tube as input and mixed with 10 μl of protein loading dye (LD) 4×. For RNA-free pulldowns, 5 μl of H_2O were added. For RNA-pulldown assays, 1 μl of H_2O, 2 μl of 10 mM 3′ biotinylated 30 mer RNA (rCrGrU rCrCrA rUrCrU rGrGrU rCrArU rCrUrA rGrUrG rArUrA rUrCrA rUrCrG, ordered from IDT), and 2 μl of 50 μM ADPNP or ATP were added. The samples were complemented with 30 μl of Binding Buffer 2× (40 mM Hepes pH 7.5, 87 mM NaCl, 4 mM MgAc2, 4 mM imidazole, 0.2% NP-40, 4 mM DTT, and 4 mM CaCl2 if CBP pulldown) and incubated for 20 min at 30°C. For CBP pulldowns assays, 15 μl of Calmodulin Sepharose 4B resin (50% Slurry, GE Healthcare) were added. For RNA-pulldowns, 5 μl of preblocked Streptavidin Dynabeads My-One (Thermo Fisher) were added. Beads were preblocked with 40 μl of 5 M NaCl, 2.5 μl of Glycogen Carrier (2 mg/ml), 5 μl of transfer RNA (tRNA) yeast (10 mg/ml), and 50 μl of bovine serum albumin (BSA) (10 mg/ml). The samples were completed with Binding Buffer 1× (20 mM Hepes pH 7.5, 125 mM NaCl, 2 mM MgAc2, 2 mM Imidazole, 0.1% NP-40, 2 mM DTT, and 2 mM $CaCl_2$ if CBP pulldown) to make a total volume of 200 μl and incubated for 1 h at 4°C with rotation. The beads were washed three times with 800 μl of Wash Buffer 1× (20 mM Hepes pH 7.5, 2 mM MgAc2, 2 mM imidazole, 0.1% NP-40, 2 mM DTT, and 2 mM $CaCl_2$, complemented with either 250 mM, 300 mM, 350 mM or 500 mM NaCl as mentioned). After each wash, samples were rotated for 2 min at 4°C, centrifuged for 30 s at 2000 rpm and 4°C. Proteins were eluted with 10 μl of LD 4× and loaded into a 15-well NuPAGE 4%–12% acrylamide SDS–PAGE (Thermo Fisher Scientific). Gels were scanned using an Eson Perfection V700 Photo scanner, and quantification of protein pulldown was performed using FIJI Gel Analyzer tool to measure the signal value of pulldown gels. Values were normalized as mentioned in figure legends and unilateral unpaired Student's *t*-tests were performed to assess statistical significance.

AlphaFold3 simulations

Five 3D structure models of *S.c.* Upf1-CH bound to Dcp2-UBM1, Dcp2-UBM2, or Upf2-Ct were generated using the seed auto option of the recently launched AlphaFold3 server (AF3; version 3.0; https://alphafoldserver.com; [53]) and the aa sequences of the proteins of interest [53, 54]. The 3D model of the *S.c.* Ebs1 protein was generated using the same approach.

Sequence alignments

Multiple sequence alignment of fungal Dcp2 proteins was obtained by performing PSI-BLAST using the sequence of *S.c.* Dcp2 [55]. The identification of the UBM1 and UBM2 motifs was facilitated by former yeast two-hybrid data that identified conserved residues in two Dcp2 regions interacting with Upf1 [56].

Electrophoretic mobility shift assay

40 pmoles of a single-stranded 30-mer oligoribonucleotide [57] was 5′end-labeled using 80 U of T4 polynucleotide kinase (New England Biolabs) and 10 fmoles of α^{32}P-ATP (3000 Ci/mmole, Perkin Elmer). Electrophoretic mobility shift assay (EMSA) samples were prepared by mixing 4 nM of the radiolabeled RNA with the indicated concentrations of proteins, with or without ADPNP or ATP (1 mM) in a buffer containing 20 mM MES pH 6.0, 100 mM potassium acetate, 2 mM DTT, 0.2 mg/ml of BSA, and 6% (v/v) glycerol. The 10 μl of reaction mixtures were incubated at 30°C for 20 min before incubation on ice and addition of 1 μl of loading dye [0.05% xylene cyanol, 0.05% bromophenol blue, and 10% (v/v) glycerol]. Half of the samples were loaded on a 0.8 mm thick native 7% polyacrylamide (29:1) gel containing 0.5% TBE. Electrophoresis was run for 2.5 h, constant voltage (240 volts) before exposure of the gel at −50°C and analysis by phosphorimaging (Typhoon FLA 9000 gel imager, GE).

Fluorescence anisotropy

N-terminally FITC-labeled Dcp-UBM1 (aa 456–479) and Dcp-UBM2 (aa 694–718) peptides were purchased from Proteogenix. Quality and purity of the final products were assessed by HPLC and mass spectrometry.

Fluorescence anisotropy measurements were performed using a FP8300 spectrofluorimeter (Jasco) at 20°C. Excitation and emission wavelengths were 495 and 520 nm, respectively. Excitation and emission slits were set-up at 2.5 and 5 nm, respectively. Response time was set to 1 s. Each anisotropy value corresponds to the mean value obtained from 15 measurements.

Binding curves were determined by titrating the fluorescent peptides with increasing amounts of CBP-Upf1-CH-His (0–40 μM) or CBP-His-ZZ (0–35 μM) into a solution composed of 20 mM HEPES pH 7.5, 125 mM NaCl and 2 mM MgAcetate and containing the respective fluorescent Dcp2-UBM peptide (UBM) at a concentration of 15 nM in a 700 μl final volume. Kd_{UBM} and dR_{max} (maximum value of anisotropy difference) were calculated by fitting experimental curves with equation (1) using the program OriginLabs:

$$dR = \left(dR_{max} * [Upf1 - CH]\right) / (KdUBM + [Upf1 - CH]) \quad (1)$$

where dR is the anisotropy difference for a given Upf1-CH concentration [Upf1-CH].

For competition experiments, the fluorescent Dcp2-UBM2 peptide (15 nM) was first incubated with CBP-Upf1-CH-His (20 μM) and then titrated with increasing concentrations of Upf2-Cter. Dissociation constant ($Kd_{Upf2\text{-}Cter}$) was determined by fitting the experimental curve with equation (2):

$$dR = ((dR_{max} - dR_{min}) * [Upf1 - CH])/([Upf1 - CH] + Kd_{UBM2}(([Upf2 - Cter]/Kd_{Upf2-Cter}) + 1))) + dR_{min} \quad (2)$$

where dR is the anisotropy difference for a given concentration of unlabeled Upf2-Cter [Upf2-Cter].

Results

Dcp2 directly interacts with Upf1 N-terminal CH domain

S.c. Upf1 is a 971 amino acid (aa) protein composed of three main domains (Fig. 1A): an N-terminal domain rich in cysteine and histidine (CH, aa 54–220), followed by the SF1 helicase domain (HD, aa 221–851), and a less conserved and poorly structured C-terminal region (Ct, aa 852–971). To study the interaction between Upf1 and the components of the decapping complex, we purified several versions of Upf1 recombinant proteins from *E. coli*, including the full-length (FL) protein Upf1 (Upf1-FL) and truncated versions (Fig. 1A). Each version of Upf1 was fused to an N-terminal calmodulin-binding peptide (CBP) used for pulldown assays. The N-terminal domain of *S.c.* Dcp2 (970 aa) bears the decapping Nudix domain flanked by an N-terminal regulatory domain (NRD) required for Dcp1 recruitment [58] and a short domain that mediates the interaction with its activator Edc3 [48, 59] (Fig. 1B). Within the long unstructured C-terminal domain reside several direct or indirect binding sites for decapping regulatory factors including Edc3, Pat1 and two potential UBMs [47, 56, 60]. These domains were mapped between aa 434–508 for UBM1 and between aa 687–720 for UBM2 (Fig. 1B). We purified a short glutathione-S-transferase (GST)-tagged version of Dcp2 encompassing both UBMs (GST-Dcp2-UBM, aa 434–720) and a longer His-tagged version (Dcp2-L, aa 1–720) that required the coexpression with full-length GST-Dcp1 for efficient purification [48] (Fig. 1B). For binding assays, we mixed different combinations of recombinant proteins, and interactions were detected by copurification on calmodulin resin in the presence of Ca^{2+}. After extensive washing at high salt concentrations (250 or 500 mM), the eluted proteins were fractionated by SDS–PAGE and directly visualized by Coomassie Blue staining (see "Materials and methods" section).

We first verified that none of the different CBP-Upf1 constructs interacted with the GST tag (Supplementary Fig. S1A). We observed that the isolated Upf1-CH protein formed an SDS-resistant dimer (Supplementary Fig. S1A, lane 3) identified using Western blotting and mass spectrometry analyses. This dimer became enriched during the pulldown assay. When CBP-Upf1 proteins were used as bait, Dcp2-UBM was efficiently coprecipitated with all CH-bearing constructs of Upf1 (Fig. 1C, lanes 2–4) but not by the constructs lacking the CH domain (Fig. 1C, lanes 5–7). Consistently, the heterodimer Dcp1/Dcp2-L was also pulled down by all the CH-bearing Upf1 constructs (Fig. 1D, lanes 2–4). When the stringency of the washing conditions was increased, the interaction was maintained (Supplementary Fig. S1B). Surprisingly, a weak but reproducible and stable interaction was detected between the isolated Upf1-HD domain and the Dcp1/Dcp2-L dimer (Fig. 1D, lane 5; Supplementary Fig. S1B, lane 5). Thus, we produced a GST-tagged full-length Dcp1 (aa 1–231) protein (Fig. 1B) and we tested the interaction with Upf1 constructs by CBP-pulldown. We observed Dcp1 coprecipitation by all CH-containing Upf1 constructs but also by the isolated HD and HD-Ct domains (Fig. 1E, lanes 2–6), indicating that Upf1 may also directly contact Dcp1 through its CH and HD domains. This result was verified using the Dcp1/Dcp2-S heterodimer in which Dcp1-FL was coexpressed with a shorter version of Dcp2 (aa 1–315), lacking the C-terminal extension which bears the UBM domains (Supplementary Fig. S1C, lanes 2–6). Collectively, these results show that Dcp2 directly and stably interacts with the CH domain of Upf1 via its C-terminal UBM-containing domain and that its cofactor Dcp1 binds the CH and HD domains of Upf1 (as summarized in Fig. 1F).

Sequence alignments of the UBM domains (UBM1 and UBM2) revealed conserved residues between the two UBM sites (Fig. 1B, and Supplementary Fig. S2A and B). Consistently, AlphaFold3 (AF3) structural prediction of the Upf1-CH domain bound to either Dcp2 UBM1 or UBM2 (Fig. 1G, and Supplementary Fig. S2C and D) showed similar binding modes and both presented high ipTM confidence scores (0.82 and 0.73, respectively) (Fig. 1G, and Supplementary Fig. S2E and F). In these models, Dcp2-UMB1 (aa 464–468) and Dcp2-UBM2 (aa 702–705) form a β-strand with one β-strand from Upf1-CH (aa 142–145). The conserved hydrophobic residues of both UBMs would similarly interact with the hydrophobic pocket within the CH domain (Fig. 1G). The predicted involvement of these hydrophobic residues at the interface is supported by the resistance of the Upf1–Dcp2 interaction to higher salt concentrations (500 mM and Supplementary Fig. S1B). To directly test the importance of this hydrophobic pocket, we replaced the four hydrophobic residues of Dcp2 with arginines (L467R, I466R, L704R, and L705R) in

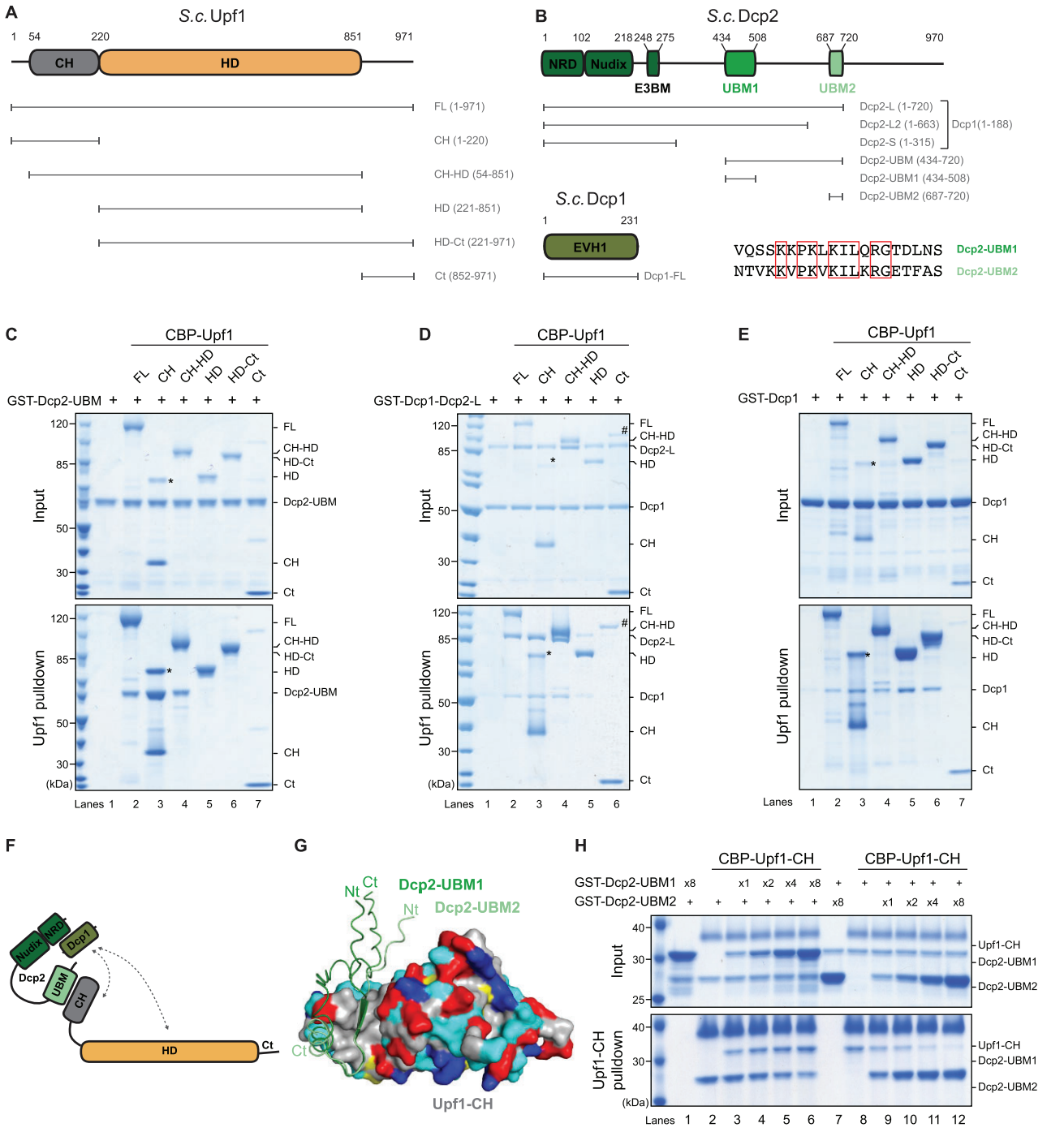

Figure 1. Decapping proteins directly interact with Upf1-CH domain. (**A**) Schematic representation of *S.c.* Upf1 domain arrangement and constructs used for pulldown assays. All constructs feature an N-terminal CBP tag and a C-terminal 6-His tag. Globular domains are depicted as ovals, while lines denote unstructured regions. (**B**) Schematic representation of *S.c.* Dcp2 and Dcp1 constructs used for pulldown assays. Dcp2-UBM (434–720) encompasses both UBMs UBM1 and UBM2 whereas isolated Dcp2-UBM1 and UBM2 correspond to truncations 434–508 and 687–720, respectively. All truncations bear a GST tag in N-terminus. The heterodimers Dcp1/Dcp2-L and Dcp1/Dcp2-L2 were coexpressed and fused to an N-terminal GST tag on Dcp1 (1–188) and a C-terminal 6-His tag on Dcp2-L or Dcp2-L2 (aa 1–720 or aa 1–663, respectively. Sequence alignment of UBM1 and UBM2 obtained using SEAVIEW [89]. Conserved residues are indicated by red squares. (**C**–**E**) CBP-pulldown assays using Upf1 truncations against Dcp2-UBM (C), Dcp2-L/Dcp1 (D), and Dcp1 (E). Protein mixtures before (input, 17% of total) or after precipitation (pulldown) were separated on SDS–PAGE and revealed using Coomassie blue. Precipitates were washed with a solution containing 250 mM NaCl, except if noted otherwise. Protein contaminants are indicated with (#). The band indicated with (*) corresponds to a stable dimerization of the isolated CH domain, which has been identified by mass spectrometry and by western blotting. (**F**) Schematic representation of protein–protein interactions between Upf1, Dcp2, and Dcp1. (**G**) Superposition of AlphaFold3 models of the *S.c.* Upf1-CH domain (colored according to amino acid properties) bound to Dcp2-UBM1 and Dcp2-UBM2. Amino acid physicochemical properties are color coded as follows: hydrophobic residues in gray, polar residues in cyan, positively charged residues in blue, negatively charged residues in red and Cys in yellow. (**H**) CBP-pulldown competition assays using Upf1-CH as bait against Dcp2-UBM2 in excess of Dcp2-UBM1 (left) and Dcp2-UBM1 in excess of Dcp2-UBM2 (right). The excess in input of Dcp2 is marked in the top panel.

GST-Dcp2-UBM (Supplementary Fig. S2G and H). These mutations totally abolished Dcp2 interaction with Upf1-CH, supporting the AF3 model (Supplementary Fig. S2I). Since the predicted structures indicated a potential competition between both UBM domains for Upf1 binding, we purified GST-tagged isolated Dcp2-UBM1 (aa 435–508) and Dcp2-UBM2 (aa 687–720) (Fig. 1B) to test their individual binding to Upf1 and potential competition. Binding assays using the different CBP-Upf1 constructs as bait showed that each Dcp2 UBM domain was efficiently coprecipitated by all CH-bearing constructs: Upf1-FL, Upf1-CH-HD, and Upf1-CH (Supplementary Fig. S1D and E, lanes 2–4).

Given that both UBM domains were predicted to interact similarly with Upf1-CH (Fig. 1G), we next conducted competition assays by pulling down on CBP-Upf1-CH from a protein mixture containing either an excess of Dcp2-UBM1 and stable quantities of Dcp2-UBM2 or vice versa (Fig. 1H). In the presence of an excess of Dcp2-UBM1, the coprecipitation of Dcp2-UBM2 by CBP-Upf1-CH slightly decreased (Fig. 1H, lanes 3–6; Supplementary Fig. S1G and H). In the reverse case, Dcp2-UBM1 coprecipitation was highly reduced in excess of Dcp2-UBM2 (Fig. 1H, lanes 9–12; Supplementary Fig. S1G and H). This suggests that both UBM1 and UBM2 bind the same surface of Upf1-CH and can displace each other, with UBM2 having a stronger effect. However, when in excess, both UBM domains were bound by Upf1 similarly (Supplementary Fig. S1H). No effect on either Dcp2-UBM1 or Dcp2-UBM2 binding was detected when incubating with increasing quantities of GST-tag protein (Supplementary Fig. S1F). Next, we quantified the affinity between CBP-Upf1-CH and fluorescently labeled peptides corresponding to either Dcp2-UBM1 (aa 456–479) or Dcp2-UBM2 (aa 694–718) by fluorescence anisotropy. We measured the anisotropy difference between each peptide free in solution or incubated with various concentrations of CBP-Upf1-CH to determine *K*d values (Supplementary Fig. S1I). Since the amount of CBP-Upf1-CH was limiting, saturation could not be reached. However, CBP-Upf1-CH binds UBM1 and UBM2 with approximate *K*d of 60.1 μM and 25.1 μM, respectively, corroborating our observations that UBM2 has a moderate stronger effect than UBM1 in our competition assays (Fig. 1H, and Supplementary Fig. S1G and H).

In agreement with the predicted AF3 structures, this demonstrates that both Dcp2 UBM domains compete for the same binding site on Upf1-CH and that UBM2 has a higher affinity for Upf1.

Multiple interactions between Upf1-decapping complex components

In addition to the decapping enzyme, the Upf1-decapping complex also contains the NMD-associated factors Nmd4 and Ebs1 and the decapping activator Edc3. *In vivo* coprecipitation experiments showed the importance of HD and Ct domains of Upf1 for the binding of Nmd4 and Ebs1, respectively [45]. Nmd4 contains an N-terminal PIN domain (aa 1–168) similar to that of the human endonuclease Smg6 and Smg5, followed by a short disordered C-terminal arm [45, 61] (Fig. 2A). The 3D model of Ebs1 predicted by AF3 (Supplementary Fig. S3A) supports a globular architecture for aa 1–591 flanked by a disordered C-terminal region (aa 592–884) predicted with low pLDDT values [62–64]. The structured 1–591 domain is composed of an N-terminal 14–3-3 domain similar to that of the human Smg5/Smg7 proteins [65] associated with a large helical hairpin subdomain, similar to Est1 [45]. We purified full-length Nmd4 (aa 1–218) fused to an N-terminal twin-strep (TS) tag, and a soluble version of Ebs1 with a deletion of the last disordered 293 aa (Ebs1, aa 1–591) fused to an N-terminal GST tag (Fig. 2A). We first mixed individually Nmd4 and Ebs1 with the different versions of CBP-Upf1. Nmd4 was coprecipitated by all Upf1 versions except Upf1-Ct (Supplementary Fig. S3B) validating that it directly interacts with the helicase domain of Upf1, as previously suggested [45]. Additionally, Nmd4 also coprecipitated with the CH domain of Upf1 (Supplementary Fig. S3B, lane 3). To what extent the contacts of Nmd4 with both the CH and HD domains contribute to the interaction of Upf1 with Nmd4 remains unknown. Furthermore, we observed a direct interaction of Ebs1 with Upf1 that is mainly mediated by the C-terminal domain of Upf1, as Ebs1 was efficiently precipitated by Upf1-FL and Upf1-Ct (Supplementary Fig. S3C, lanes 2 and 5, Fig. 2B for a schematics of observed interactions). We did not include Edc3, as we could not recapitulate stable interactions with other components of the decapping complex in our experimental conditions.

We next evaluated whether the individual interactions of Dcp2, Nmd4, and Ebs1 with Upf1-FL interfered with each other. To differentiate each protein and enhance the solubility of Ebs1, we generated HisSUMO-tagged Ebs1 (aa 1–591). CBP-Upf1-FL was mixed with either one partner, a combination of two partners, or all three partners and used as bait (Fig. 2C). Upf1-FL precipitated its partners both individually and in combination, indicating no interference among the interactions (Fig. 2C, lanes 5–7). To verify our findings, we conducted a similar experiment using GST-Dcp2-UBM as bait (Fig. 2D). Dcp2-UBM coprecipitated Upf1-FL but not Nmd4 or Ebs1, whether alone or together (Fig. 2D, lanes 2, 4, and 6). In contrast, Dcp2-UBM coprecipitated Nmd4 and/or Ebs1 only in the presence of Upf1-FL (Fig. 2D, lanes 5, 7, and 8). This demonstrated the successful reconstitution of the tetrameric complex even if we cannot exclude a mixture with the trimeric complexes: Upf1–Dcp2–Nmd4 and Upf1–Dcp2–Ebs1 (Fig. 2D).

To further investigate the network of interactions among the components of the Upf1-decapping complex we performed GST-pulldowns using the GST-Dcp1/Dcp2-L heterodimer as bait (Supplementary Fig. S3D). Despite the fact that in our experimental conditions, the heterodimer Dcp1/Dcp2 shows a weak stability, we observed that Dcp1/Dcp2 directly interacted with Upf1-FL and Ebs1 individually (Supplementary Fig. S3D, lanes 3 and 4). In agreement with our previous pulldowns, Nmd4 was only coprecipitated in the presence of Upf1 and all three proteins were coprecipitated by GST-Dcp1/Dcp2-L when mixed together (Supplementary Fig. S3D, lane 8). We further explored the interactions between Nmd4, Dcp1/Dcp2 and Ebs1 in the absence of Upf1, the keystone of the complex. We used CBP-Nmd4 or CBP-Ebs1 as bait against GST-Ebs1 and HisZZ-Nmd4 respectively (Fig. 2E) and observed a weak but consistent interaction between Nmd4 and Ebs1. Furthermore, we produced a shorter and more stable GST-tagged Dcp2 truncation (aa 1–663) containing UBM1 (Dcp2-L2) (Fig. 1B) and used CBP-Ebs1 as bait. We observed a weak but reproducible interaction of Ebs1 with the heterodimer Dcp1/Dcp2-L2 and the isolated Dcp1 protein but not with Dcp2-UBM (Fig. 2F) supporting a direct interaction between Ebs1 and Dcp1 and

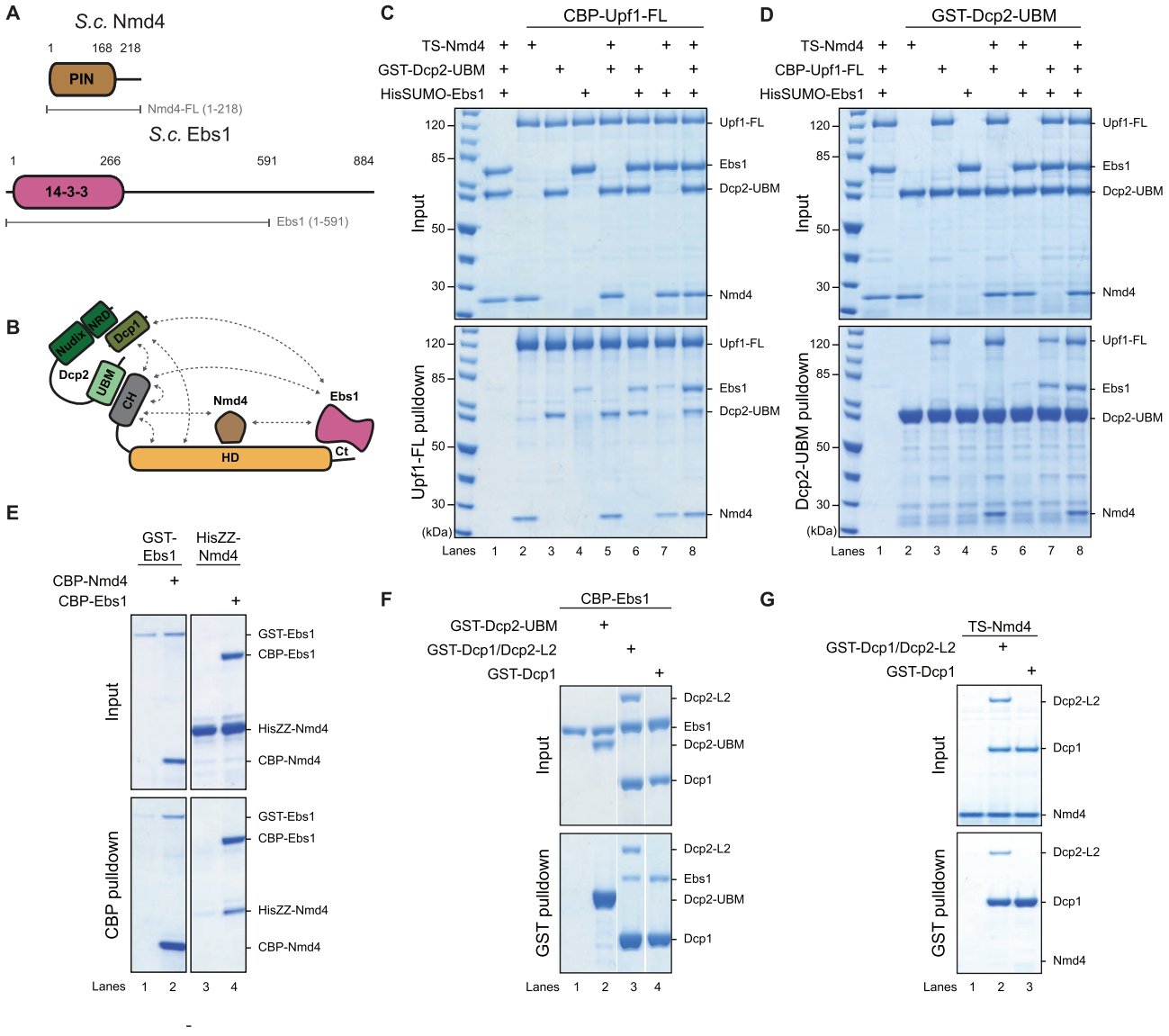

Figure 2. Multiple interactions between Upf1 decapping complex components. (**A**) Schematic representation of *S.c.* Nmd4 and Ebs1 constructs used for pulldown assays. Multiple fusion proteins were produced, with Nmd4-FL (aa 1–218) fused at the N-terminus to either a Twin Strep (TS) tag, CBP, HisZZ, or left untagged. The globular domain of Ebs1 (aa 1–591) was fused at the N-terminus to GST, CBP, or His-SUMO tags. (**B**) Schematic representation of protein–protein interactions between Upf1, Dcp2, Dcp1, Nmd4, and Ebs1. (**C**) CBP-pulldown assays using Upf1-FL against combination of Nmd4-FL, Ebs1 (1–591), and Dcp2-UBM as indicated. As previously, protein mixtures before (input, 17% of total) or after precipitation were separated on SDS–PAGE and revealed using Coomassie blue. Protein contaminants are indicated with (#). (**D**) GST-pulldown assays using Dcp2-UBM as bait against combination of Nmd4-FL, Ebs1 (1–591), and Upf1-FL as indicated. (**E**) CBP-pulldown assay using CBP-Nmd4 as bait against GST-Ebs1 (left) and CBP-Ebs1 against HisZZ-Nmd4 (right). (**F** and **G**) GST-pulldown assays using Dcp2-UBM, Dcp1-FL/Dcp2-L2 or isolated Dcp1-FL as bait against CBP-Ebs1 (F) or TS-Nmd4 (G).

consistent with previous two hybrid results [66]. This interaction was confirmed by reverse CBP pulldowns with the same proteins (Supplementary Fig. S3E). However, we did not detect direct interactions between Dcp1, Dcp2, and Nmd4 (Fig 2G and Supplementary Fig. S3F). Together, these experiments revealed an intricate network of interactions within the Upf1-decapping complex (summarized in Fig. 2B).

Yeast Upf1–Upf2 interaction is homologous to the human one

The three core NMD factors Upf1, Upf2, and Upf3 form a trimeric complex [45] that assembles during, or rapidly after, PTC recognition. The overall organization of the Upf complex appears to be conserved, with Upf2 bridging Upf1 and Upf3 [20, 45, 67]. Upf2 is composed of three MIF4G domains, the third of which binds Upf3 [68–70], followed by a disordered C-terminal region containing the UBM (aa 933–1089, Fig. 3A). In humans, Upf2 has been reported to stimulate the helicase and ATPase activity of Upf1 [16]. The crystal structure of human Upf1/Upf2 showed that Upf2 binds the CH domain in a bipartite manner, binding one side of the CH domain via a β hairpin and the other side via an α helix [71]. The combination of both binding sites renders a highly stable interaction with low dissociation constants [71]. We modeled the yeast Upf1-CH interaction with Upf2-Ct using AF3 [53] (Fig. 3B). The model confidently predicted a similar bipartite mode of interaction in which yeast Upf2 would also clamp op-

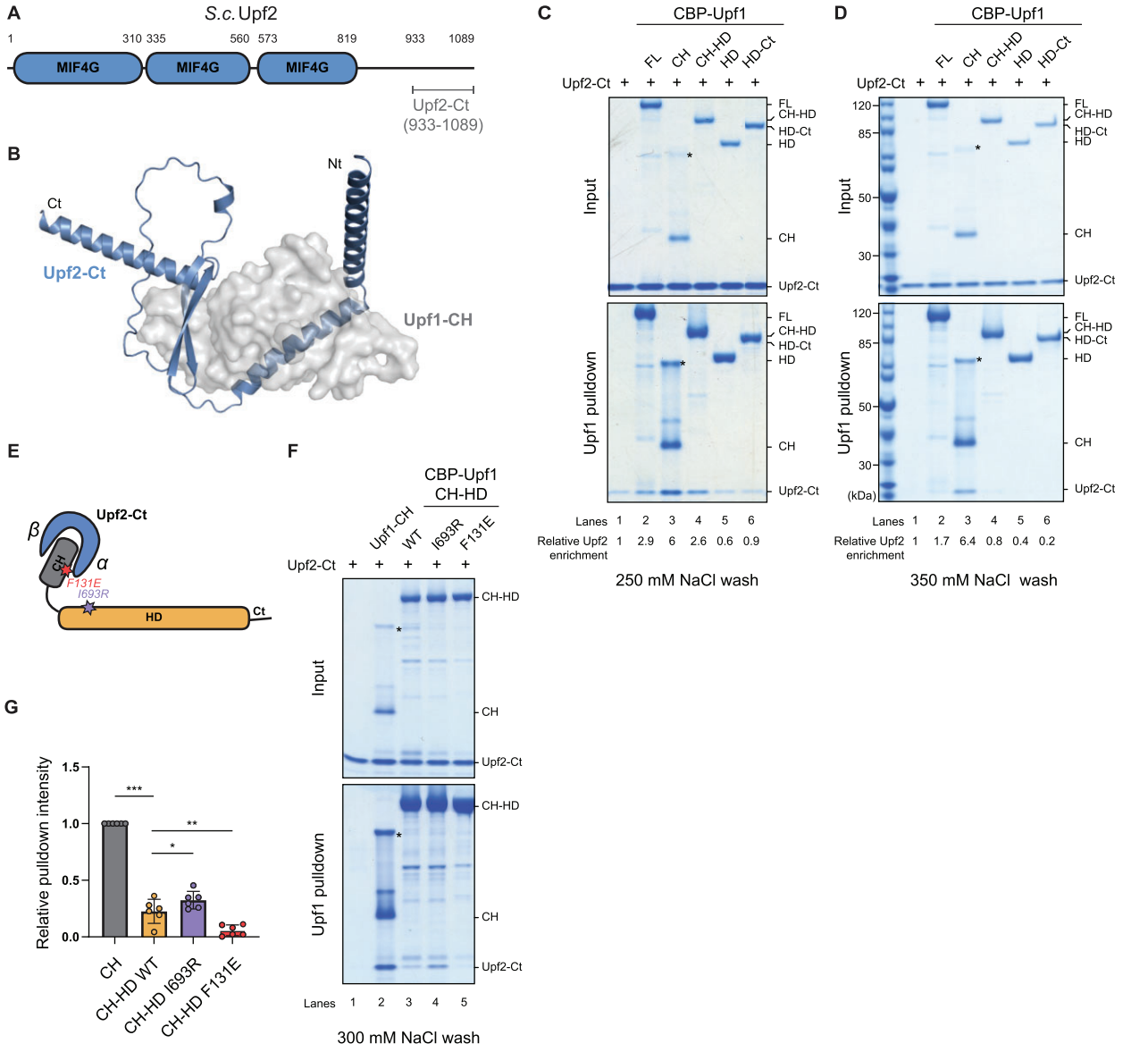

Figure 3. Direct interaction of Upf2 with Upf1 CH domain. (**A**) Schematic representation of *S.c.* Upf2 construct used for pulldown assays. Upf2-Ct (933–1089) is tagged with 6-His in C-terminus. (**B**) Representation of the best AF3 model of the interaction between Upf1-CH domain (surface shown as semi-transparent) and Upf2-Ct domain. (**C** and **D**) CBP-pulldown assays using Upf1 truncations against Upf2-Ct washed with solution containing either 250 mM NaCl (C) or 350 mM NaCl (D). As previously, protein mixtures before (input, 17% of total) or after precipitation were separated on SDS–PAGE and revealed using Coomassie blue. CH dimer is indicated with (*) and protein contaminants with (#). (**E**) Schematic representation of protein–protein interactions between Upf1 and Upf2. Mutations used in this study of important residues for the intramolecular interaction between CH and HD of Upf1 are depicted as stars. (**F**) CBP-pulldown assays using Upf1-CH, Upf1-CH-HD WT, Upf1-CH-HD I693R, or Upf1-CH-HD F131E against Upf2-Ct. (**G**) Relative band intensity quantification of Upf2 pulldown by Upf1-CH-HD WT, Upf1-CH-HD I693R or Upf1-CH-HD F131E (F), normalized by Upf2 signal intensity pulled down by Upf1-CH (F, lane 2). Error bars denote standard deviations between replicates ($n = 6$). Individual measurements are represented as circles, while the mean of each data series is represented as a column. Unpaired Student's *t* tests were performed to calculate *p* values with a significance threshold set at 0.05 marked with one star; $^{**}P < 0.01$ and $^{***}P < 0.001$.

posite sides of the CH domain with a β hairpin and an α helix (Fig 3B; Supplementary Fig. S4A and B). To study the interaction of yeast Upf1 and Upf2 *in vitro*, we purified a truncated version of Upf2 corresponding to the predicted UBM (aa 933–1089, Upf2-Ct) [16, 20] (Fig. 3A). CBP-pulldown assays with the different versions of CBP-Upf1 showed a direct interaction between Upf1-FL, Upf1-CH-HD, Upf1-CH, and Upf2-Ct (Fig. 3C), confirming the direct interaction of Upf2 with the Upf1 CH domain. The coprecipitation of Upf2-Ct by CBP-Upf1-FL and CBP-Upf1-CH-HD seemed weaker than the coprecipitation by the isolated CH domain (Fig. 3C, compare lanes 2 and 4 to lane 3) as they were slightly above background noise signal. This apparent difference was exacerbated when increasing the stringency of the washes (Fig. 3D, lanes 2 and 4), suggesting that the presence of the Upf1 helicase domain interferes with Upf2 binding.

To validate the model of Upf1–Upf2 interaction and better understand our results we tested the effect of mutating key amino acid residues. The yeast Upf1-CH-HD protein adopts a closed conformation in which the CH domain is buried within the helicase RecA2 and stalk domains when bound to RNA [16]. Such closed conformation is compatible with the bind-

ing of Nmd4 and Dcp2-UBM1 or Dcp2-UBM2 but not with Upf2 binding (Supplementary Fig. S4C and D). In this structure, the residue I693 in the RecA2 domain interacts with the F131 residue located on the surface of the CH domain (Fig. 3E). In humans, the corresponding residue (F192), is involved in the interaction with the α helix of Upf2 [16]. To investigate whether the yeast interactions followed the same mechanism, we produced CBP-Upf1-CH-HD carrying the I693R or F131E mutations (Fig. 3E), which are both expected to prevent the closed conformation of Upf1. The I693R mutation partially restored the coprecipitation of Upf2-Ct by CBP-Upf1-CH-HD under stringent washing conditions (Fig. 3F and G, compare lanes 3 and 4). As expected, the mutation F131E abolished the interaction with Upf2-Ct (Fig. 3F and G, lane 5). These results indicate that the same residues are implicated in Upf2 interaction in yeast and humans and confirmed that the intramolecular interaction between the RecA2/Stalk domains of the HD domain and the CH domain of Upf1 hampers binding of Upf2 most likely because only the β hairpin binding site is accessible [71].

Dcp2 and Upf2 compete for interaction with Upf1

Both Upf2 and Dcp2 directly interact with the CH domain of Upf1 (Figs 1 and 3). To explore whether these two Upf1 partners contact the same binding sites, we superposed the AF3 predictions of Upf1-CH/Dcp2-UBM1 and Upf1-CH/Dcp2-UBM2 with the human Upf1-CH/Upf2-Ct crystal structure [71] (PDB: 2WJV, Fig. 4A). The UBM domains of Dcp2 interact with the outer part of the CH domain in a position similar to that of Upf2's β hairpin (Fig. 4A). This steric clash suggests that Dcp2 and Upf2 cannot simultaneously bind the Upf1 CH domain (Fig. 4B). To test this hypothesis biochemically, we conducted competition assays by pulling down CBP-Upf1-CH from a protein mixture containing a fixed amount of Upf2-Ct with gradually increasing quantities of Dcp2-UBM (Fig. 4C). The presence of two to eight times more Dcp2-UBM reduced the amount of Upf2 coprecipitated by Upf1-CH (Fig. 4C, lanes 2–6, and Supplementary Fig. S5A, blue). However, coprecipitation of Dcp2-UBM only marginally increased when used in excess (Fig. 4C, lanes 3–6, and Supplementary Fig. S5B, green) showing an almost stoichiometric binding. The reverse experiment, in which the amount of Dcp2-UBM was constant while the amount of Upf2-UBM increased, led to a comparable reduction of Dcp2-UBM (Fig. 4D, lanes 2–6, and Supplementary Fig. S5A, green) but a further increased amount of Upf2-Ct was coprecipitated when in excess (Fig. 4D, lanes 3–6, and Supplementary Fig. S5B, blue). To confirm the competition between the two partners, we performed sequential binding assays (Fig. 4E). We mixed CBP-Upf1-CH with a saturating amount of Dcp2-UBM (Fig. 4E, lane 1), washed away the unbound excess of Dcp2-UBM and then added increasing amounts of Upf2-Ct (Fig. 4E, lanes 2–5). The latter progressively displaced Dcp2-UBM as previously observed (compare Fig. 4D and 4E). In contrast, when Upf1-CH was saturated with Upf2-Ct (Fig. 4E, lane 6) before addition of Dcp2-UBM (Fig. 4E, lanes 7–10), its displacement was limited (compare Fig. 4C and 4E). Our results suggest that Upf2 and Dcp2 compete for the same binding site on the Upf1-CH domain, but that the bipartite interaction of Upf2 with the CH domain offers a more stable grip than that of Dcp2. This was confirmed by anisotropy fluorescence measurements, which allowed to determine a K_d of CBP-Upf1-CH for Upf2-Ct. We first incubated CBP-Upf1-CH with the fluorescently labeled Dcp2 UBM2 (aa 694–718) peptide and then titrated with increasing concentrations of Upf2-Ct. Due to the competition between Upf2-Ct and Dcp2 UBM2 for interaction with CBP-Upf1-CH, the displacement of Dcp2 UBM2 by Upf2-Ct results in a decrease in fluorescence anisotropy, from which we could calculate a K_d value of 0.43 μM for the interaction between CBP-Upf1-CH and Upf2-Ct (Fig. 4F). This value is ∼140 and 60 times lower than those determined for Dcp2 UBM1 and Dcp2 UBM2 peptides, respectively. This K_d between yeast proteins is very similar to one previously measured between human proteins [71].

Consistent with our previous data showing that the Upf1-2/3 and Upf1-decapping complexes purified from yeast are mutually exclusive [45], our results suggest that this incompatibility is, at least partly, due to the competition between Upf2 and Dcp2 for interaction with Upf1-CH. This could also be due in part to a steric clash observed between yeast Nmd4 and human Upf1-CH domain clearly observed when superposing the crystal structure of yeast Nmd4/Upf1-HD onto the crystal structure of the human Upf1-CH-HD/Upf2-Ct (Supplementary Fig. S5C).

Upf1 RNA-binding is differentially regulated by its partners

To evaluate the ability of Upf1-FL to bind RNA in the presence or in the absence of its NMD partners, we performed RNA-pulldown assays. As for the protein interaction assays, the proteins were first mixed in the presence of a short (33 mer) 3′-end biotinylated RNA with or without ATP or ADPNP, a nonhydrolysable analog of ATP before purification on streptavidin beads. As previously observed [16, 19, 72], Upf1 binding to RNA differed in the presence or absence of ATP. Upf1-FL was better retained by the RNA in the absence of nucleotide or in the presence of ADPNP, a non-hydrolysable analog ATP, than in the presence of ATP (Fig. 5A, lanes 2, 6, 10). Due to unspecific interactions between all tested Ebs1 versions and the streptavidin resin, we did not include this protein in these RNA-pulldown experiments. Moreover, since the TS-tagged version of Nmd4 presented unspecific interactions with the resin, we purified a His-tagged version of Nmd4. In contrast to Nmd4 that was slightly pulled down by RNA, neither Dcp2-UBM nor Upf2-Ct were individually retained by the RNA (Fig. 5A, lane 1). The addition of Upf2-Ct reduced the amount of Upf1 retained by the RNA by half (Fig. 5A and B, lanes 5 and 9 for quantification). This was particularly visible in the absence of nucleotide or in the presence of ADPNP when Upf1 recovered by RNA purification was the most important, suggesting that Upf2 prevents Upf1 binding to RNA (Fig. 5A). Regardless of the condition, Upf2-Ct was never coprecipitated by the RNA in the presence of Upf1 (Fig. 5A), in agreement with structural data (Supplementary Fig. S5C). Remarkably, we observed an opposite effect when testing two components of the Upf1-decapping complex. The addition of Nmd4 and, to a lesser extent, Dcp2-UBM, significantly increased the amount of Upf1 retained by RNA in the presence of ADPNP or ATP (Fig. 5A and B, lanes 7, 8, 11, and 12). This positive effect was not measurable in the absence of nucleotide as Upf1 was already strongly attached to RNA (Fig. 5A and B, lanes 3 and 4). In contrast to Upf2-Ct, it is noteworthy that Dcp2-UBM and Nmd4 systematically coprecipitated with the RNA-bound Upf1 in all conditions. Therefore, individually,

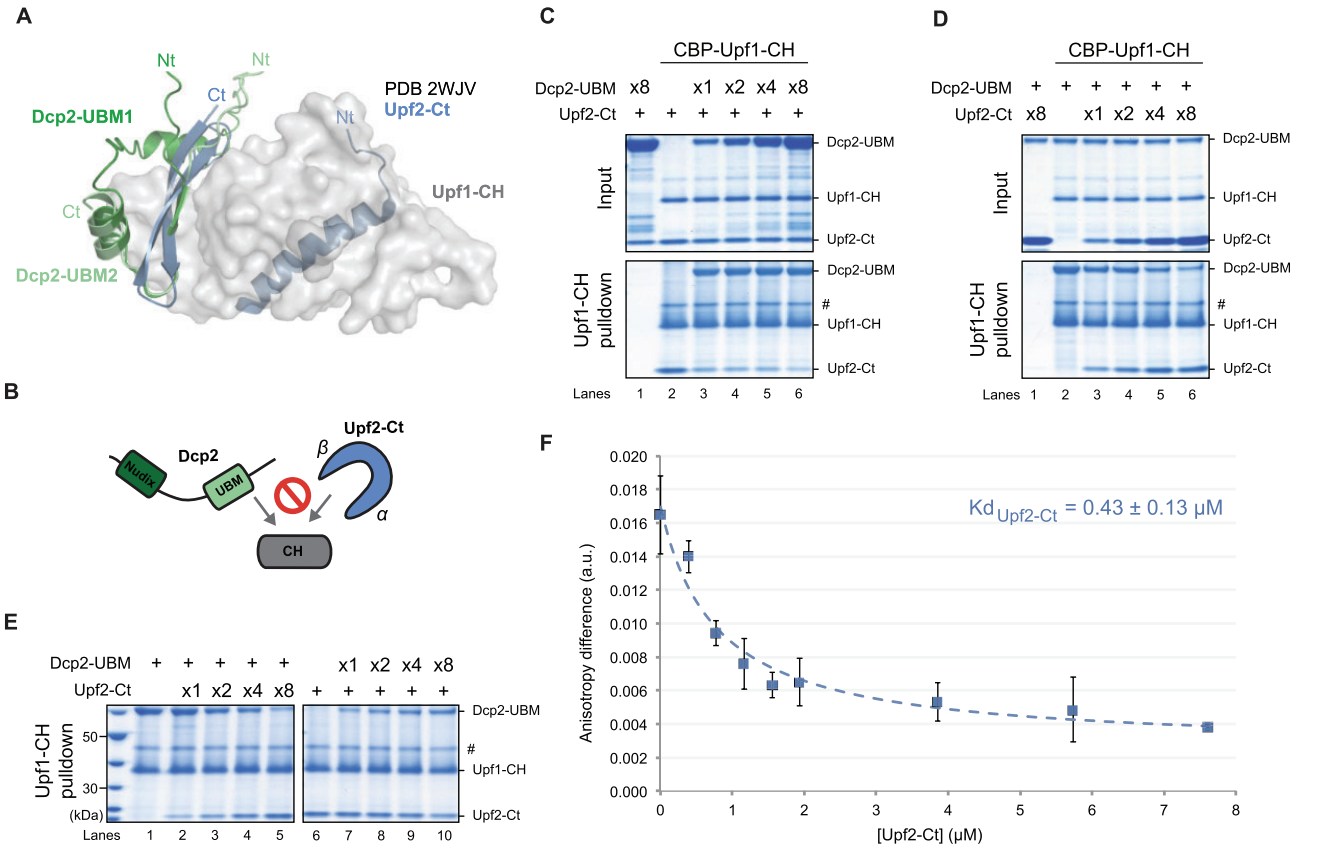

Figure 4. Upf2 and Dcp2 compete for binding to Upf1-CH domain. (**A**) Superposition of the best AF3 models of the *S.c.* Upf1-CH domain (shown as semi-transparent) bound to Dcp2 UBM1 and UBM2 onto the crystal structure of human Upf1/Upf2 complex [62] (PDB code: 2WJV). For the sake of clarity, only yeast Upf1-CH is shown, the human Upf1 CH-HD is not shown. (**B**) Schematic representation of interaction incompatibility between Dcp2 and Upf2 binding to the CH domain of Upf1. (**C** and **D**) CBP-pulldown assays using Upf1-CH against an increasing amount of Dcp2-UBM- with a constant amount of Upf2-Ct (C) or increasing amount of Upf2-Ct with a constant amount of Dcp2-UBM (D). As previously, protein mixtures before (input, 17% of total) or after precipitation were separated on SDS–PAGE and revealed using Coomassie blue. Protein contaminants are indicated with (#). (**E**) CBP-pulldown assays using pre-formed Upf1-CH/Dcp2-UBM complex against increasing amounts of Upf2-Ct (left) or pre-formed Upf1-CH/Upf2-Ct complex against increasing amounts of Dcp2-UBM (right). (**F**) Chase experiments of FITC-labeled Dcp2-UBM2 peptide (15 nM) bound to CBP-Upf1-CH-His (20 µM) by Upf2-Cter. The curve obtained after fitting of the experimental data with equation (B) from the "Materials and methods" section is shown as a dashed black line. Error bars were calculated from triplicate experiments.

both Dcp2 and Nmd4 stabilize Upf1 bound to RNA. We performed a similar experiment in the presence of ATP by mixing Upf1-FL with either partner, a combination of two partners or all three partners simultaneously (Fig. 5C). The most effective retention of Upf1-FL onto RNA was observed in the presence of both Dcp2-UBM and Nmd4, indicating their synergistic contribution to the stability of this complex, with their effects being additive (Fig. 5C and D, lanes 5, 8, and 9). Upf2-Ct showed no significant effect on the retention of Upf1-FL when either Dcp2-UBM or/and Nmd4 were present (Fig. 5C and D). These effects were also reproducible in absence of nucleotide (Supplementary Fig. S6A) and in presence of ADPNP (Supplementary Fig. S6B).

We also performed EMSA to study Upf1 binding to RNA using a complementary approach. We incubated a 30-mer radiolabeled ssRNA with increasing concentrations of CBP-Upf1-CH-HD or CBP-Upf1-FL without nucleotide, ADPNP, or ATP. In each case, a band shift was observed upon gel electrophoresis, indicating Upf1–RNA complex formation (Supplementary Fig. S6C). As previously observed, Upf1 isoforms show more affinity to RNA in the absence of nucleotides [16, 19, 72]. We found that both in the absence of nucleotides and in the presence of ATP, increasing amounts of Upf2-Ct do not bind RNA (Fig. 5E, lanes 1 and 6), but reduced the Upf1-FL shift by half (Fig. 5E, lanes 2–5 and 7–10, Supplementary Fig. S6D), confirming that Upf2 hampers Upf1 binding to RNA in presence or absence of ATP.

Next, we tested the effect of Nmd4 and Dcp2 on Upf1-CH-HD RNA binding. EMSA with Nmd4, Dcp2-UBMs, or a control protein GST added separately, showed only a weak shift when a large excess of Nmd4 (25-fold) was added to RNA (Fig. 5G, lanes 4–6). This confirms the weak affinity of Nmd4 for RNA observed by pulldown assays (Fig. 5A and C) and previous isothermal calorimetry assays [49]. When increasing amounts of Nmd4 were added to a fixed amount of Upf1-CH-HD, Nmd4 produced a super-shift already detected at equimolar concentration with Upf1 (Fig. 5G, lanes 11–14). Addition of Dcp2 in the same range showed no super-shift of Upf1 (Fig. 5G, lanes 16–20). However, a complete and even higher super-shift was detected when both Nmd4 and Dcp2 were added (Fig. 5G, lanes 21–24), while the addition of Nmd4 and GST showed no additional shift (Fig. 5G, lanes 26–29). This specific super-shift was confirmed when an equimolar and a fixed amount of Upf1 and Nmd4 were mixed with increasing

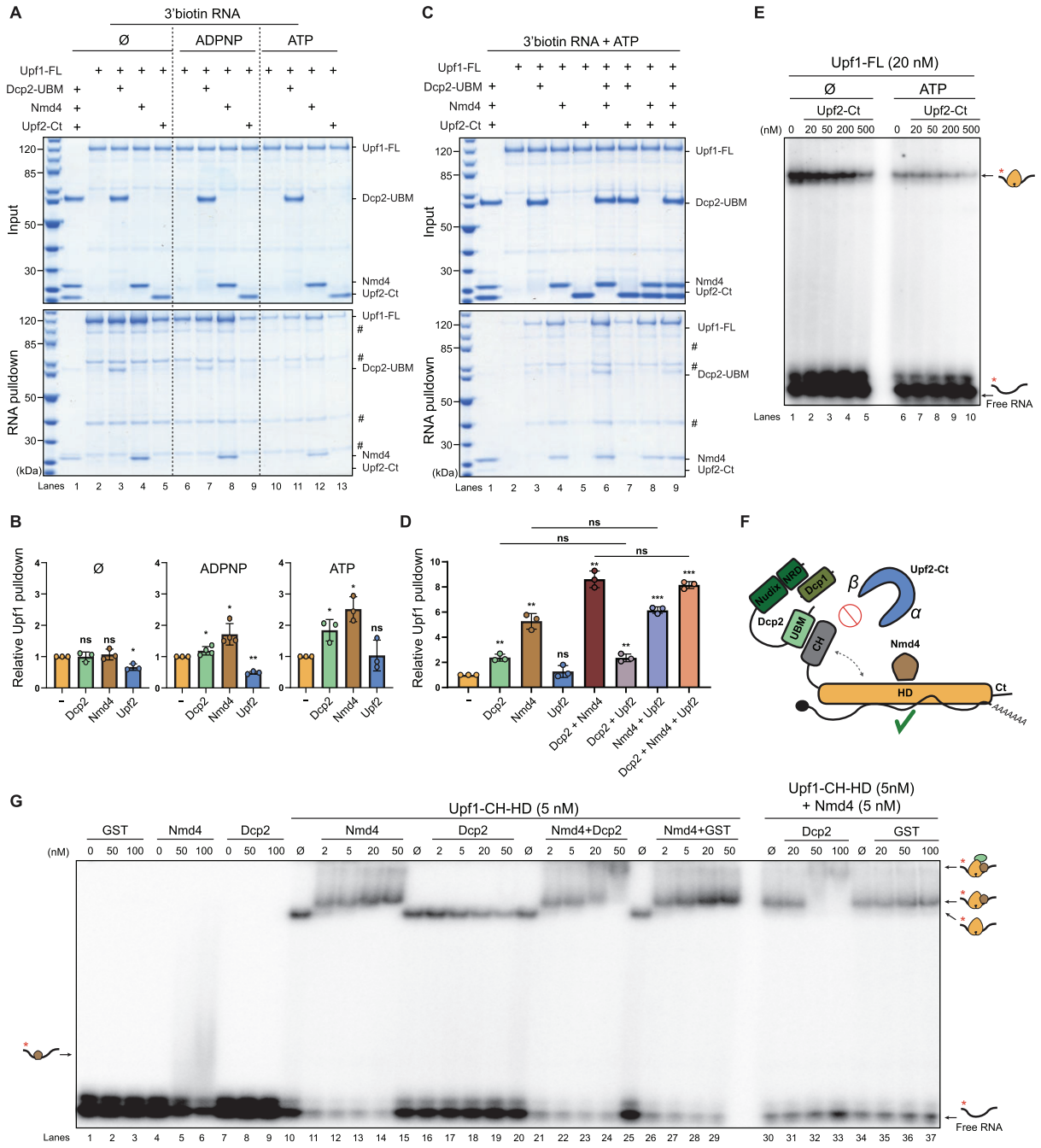

Figure 5. Upf1 RNA-binding activity is modulated by its partners. (**A**) RNA-pulldown assays using a 3′ end-biotinylated 33 mer RNA as bait. As indicated, Upf1-FL, Nmd4, Dcp2-UBM, or Upf2-Ct were mixed with the RNA in the absence of nucleotide or in the presence of ATP or ADPNP. Protein mixtures before (input, 17% of total) or after precipitation using magnetic streptavidin beads were separated on SDS–PAGE and revealed using Coomassie blue. Protein contaminants are indicated with (#). (**B**) Relative quantification of Upf1 pulldown in presence of partners (A, lower panel lanes 2–13) normalized by Upf1 pulldown without any partner (A, lower panel lanes 2, 6, or 10). Error bars denote standard deviations between replicates ($n = 3$). Individual measurements are represented as circles, while the mean of each data series is represented as a column. Unpaired *t* tests were performed to calculate *P*-values with a significance threshold set at 0.05 marked with one star. *P*-values <0.01 were marked with two stars, and <0.001 were marked with three stars. Nonsignificant *P*-values were marked with ns. (**C**) RNA-pulldown assays using a 3′ end-biotinylated 33 mer RNA as bait against Upf1-incubated with ATP and combinations of Nmd4, Dcp2-UBM, and Upf2-Ct, as indicated. (**D**) Relative quantification of Upf1 pulldown in (C) normalized by Upf1 pulldown without any partner (C, pulldown lane 2). Error bars denote standard deviations between replicates ($n = 3$). Individual measurements are represented as circles, while the mean of each data series is represented as a column. Unpaired *t* tests were performed to calculate *P*-values with a significance threshold set at 0.05 marked with one star. *P*-values <0.01 were marked with two stars, and <0.001 were marked with three stars. (**E**) Representative native 7% polyacrylamide gel illustrating the interaction of Upf1-FL (depicted in orange) with a ^{32}P-labeled 30-mer oligoribonucleotide substrate (black line with red star). The RNA substrate was incubated with 20 nM of Upf1-FL and increasing concentrations of Upf2-Ct and with (+) or without (*Φ*) ATP under the conditions described in the "Materials and methods" section. (**F**) Schematic representation of protein-RNA interactions between the Upf1, Dcp1, Dcp2, Nmd4 complex and Upf1–Upf2 complex. (**G**) Representative native 7% polyacrylamide gel illustrating the interaction of Upf1-CH-HD with a ^{32}P-labeled 30-mer oligoribonucleotide substrate (black line with red star) in presence of Dcp2-UBM, Nmd4, and/or GST as a control. The RNA substrate was incubated with 5 nM of Upf1-CH-HD and increasing concentrations of Dcp2-UBM, Nmd4 and/or GST and with ATP under the conditions described in the "Materials and methods" section.

amounts of Dcp2 but not with the GST control protein (Fig. 5G, lanes 30–37). We also observed by EMSA that the addition of a large excess of Dcp2 reduces the proportion of Upf1 bound to RNA (Fig. 5G, lanes 16–20). This clearly shows that Dcp2 alone does not favor Upf1 binding to RNA and that the recruitment of Dcp2 by Upf1 onto RNA requires Nmd4.

The EMSA results confirmed our observations from interaction assays (Fig. 5A and C). Together, these findings demonstrate that Upf1, Nmd4, and Dcp2 form a stable complex on RNA and that Upf1 and Nmd4 are necessary for stably anchoring Dcp2 onto RNA unlike Upf2, which detaches Upf1 from RNA (Fig. 5F).

Discussion

Since its discovery, genetics, functional assays, and biochemical characterization have identified most, if not all, NMD factors in different eukaryotic organisms [73]. However, the highly dynamic aspect of this process linking premature translation termination with mRNA decay challenges the characterization of the successive molecular steps. Central to NMD, Upf1 recognizes mRNAs containing PTCs and coordinates the recruitment of specific decay factors. This involves the formation of transient Upf1-containing complexes that have been only marginally characterized biochemically [45, 56, 74, 75]. Here, using isolated recombinant yeast proteins we could recapitulate critical phases of NMD and notably, direct interaction and competition between NMD and decay factors and their binding to RNA.

All three distinct domains of Upf1, the N-terminal CH domain, the central helicase domain (HD), and the disordered C-terminal domain, make direct contacts with Dcp2, Dcp1, Nmd4, and Ebs1 (Fig. 1, and Supplementary Figs S1 and S3). Interestingly, many of the partners that we included in our study directly contact distinct domains of Upf1 and other additional secondary interactions between other partners take place within the complex (Fig. 2). These findings rationalize the fact that deletion of single contact points or partners is insufficient to prevent the assembly of the complex and accounts for the weak NMD target destabilization upon individual Ebs1 and Nmd4 deletions or deletion of the C-terminal domain of Dcp2 [45, 47]. This network of interactions also explains why NMD is partially restored in a *Δupf1* yeast strain by the expression of truncated versions of Upf1 lacking the CH domain or the C-terminal domain [45]. The CH domain of Upf1 holds a pivotal position in this intricate network of interactions as it contacts all tested partners, notably the decapping protein Dcp2 and Upf1's essential cofactor Upf2. We show that Dcp2 directly interacts with Upf1 through two UBMs: UBM1 and UBM2. Mutations of conserved residues in both UBM domains abolish their interaction with Upf1 *in vitro* (Supplementary Fig. S2I). Our biochemical data and the Alphafold models presented suggest that the UBM domains contact the same hydrophobic pocket within Upf1 CH domain and that UBM2 possesses a slightly higher affinity than UBM1 from binding Upf1-CH domain (Fig. 1). Since deletion of the UBM domains scarcely impacts NMD efficacy *in vivo* [47], it remains unclear whether both UBMs contribute to the architecture of Upf1-containing decapping complexes. However, the lack of impact of UBM presence on the function of the Upf1-decapping complex can be explained by taking into consideration the previously unknown role of Dcp1, which binds directly to Upf1, as shown here (Fig. 1E).

The interactions of Dcp2 UBMs with the Upf1 CH domain are mutually exclusive with Upf2 binding (Fig. 4). Dcp2 UBMs are predicted by AF3 to contact the same external side of the CH domain that binds the β hairpin of Upf2 (Fig. 1 and Supplementary Fig. S1). Two conserved regions in Upf2, a β hairpin and an α helix, clamp two opposite sides of the Upf1 CH domain [71] (Fig. 3). This bipartite mode of interaction is therefore conserved between yeast and human [71, 76]. Interaction assays using targeted mutagenesis further confirmed this model (Fig. 3). The hydrophobic pocket of the CH domain is involved in the interaction with the Upf2 α-helix and contacts conserved residues of the RecA2 domain and the stalk—two structural elements of the helicase domain. The Upf1 I693R mutation on the surface of RecA2 favors the interaction of Upf2 most likely by giving access to both binding sites. Conversely, the F131E mutation in the hydrophobic pocket of the CH domain strongly reduces Upf2 interaction indicating the residue is involved in the interaction (Fig. 3). In human Upf1, the corresponding residue is also implicated in the interaction with Upf2 [16]. The biochemical evidence for the mutually exclusive binding of Upf1 to Upf2 or Dcp2 accounts for the two distinct Upf1-2/3 and Upf1-decapping NMD complexes isolated *in vivo* [45]. This transition between the Upf complex and the Upf1-decapping complex, which triggers mRNA decay orchestrated by the CH domain of Upf1, is most likely also conserved. In yeast, NMD targets are mainly degraded by decapping [41], making Dcp2 the main decay-inducing partner of Upf1. In human, the predominant RNA degradation pathway in NMD involves the endonucleolytic cleavage of mRNA by Smg6 [36–38, 77]. Interestingly, Upf2 and Smg6 also compete for their binding to the CH domain of Upf1 in human [78] supporting a sequential binding of these factors during NMD similar to Upf2 and Dcp2 in yeast.

Our biochemically reconstituted system allowed determining how direct partners of Upf1 influence its binding to RNA (Fig. 5). RNA-based pulldowns and EMSA experiments first showed that Upf2 reduces Upf1 binding to RNA. Yeast Upf1 HD domain contacts RNA in a closed Upf1 conformation that is controlled by the relative orientation of the CH and HD domains [16]. Docking the Upf1 CH domain onto the HD domain increases the surface contacted by RNA. This docking cannot occur when opposite faces of the CH domain are clamped by Upf2. This negative impact of Upf2 on Upf1 affinity to RNA is conserved as a similar effect occurs with the human proteins [67, 79]. Given that Upf2 bridges Upf1 and Upf3 [67], it is tempting to speculate that as part of the Upf1-2/3 complex, Upf1 is not stably attached to the RNA. Conversely, Nmd4 stabilizes Upf1 bound to RNA allowing in turn Upf1 to tether Dcp2 to the RNA. In contrast to Upf2, Dcp2 only binds the external face of the CH domain and this binding mode is compatible with the structure of yeast Upf1-CH-HD bound to RNA and ADP [16]. Dcp2 alone does not promote Upf1-RNA binding (Fig. 5). In contrast, Nmd4 promotes Upf1 RNA-binding likely by stabilizing Upf1 closed conformation. Therefore, we provide evidence of two distinct states of Upf1 regarding its binding to RNA during the stepwise NMD pathway: a poor affinity to RNA in the presence of Upf2 and its stable binding to RNA when bound to the components of the NMD-decapping complex. If the negative effect of Upf2 on Upf1 binding to RNA is conserved in human, it is tempting to believe that Upf1 also contributes to stabilize the association of the decay factors with the RNA target during the late phases of NMD.

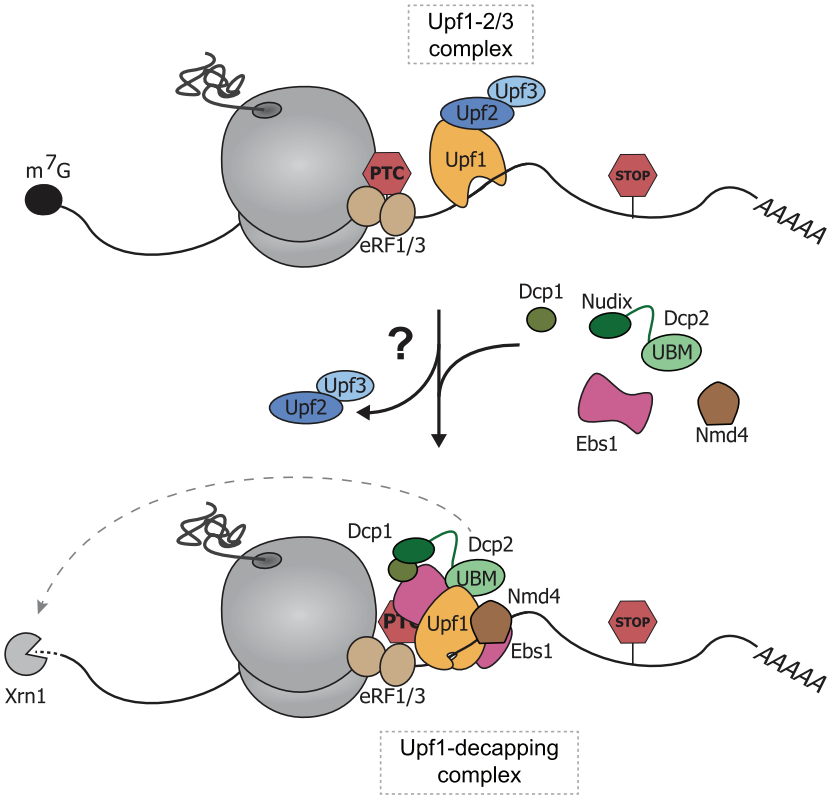

Figure 6. Proposed model for Upf1-2/3 and Upf1-decapping complex sequential formation during NMD in yeast. Upf1 is recruited to the target mRNA vicinity adjacent to the terminating ribosome, facilitated either through self-association or interaction with the ribosome within the Upf1-2/3 complex. A pivotal conformational shift ensues, facilitating Upf1 RNA-binding and the assembly of the Upf1-decapping complex, in which Nmd4 strongly stabilizes Upf1 and Dcp1/Dcp2 onto the mRNA to initiate mRNA degradation.

These biochemical snapshots of Upf1-containing complexes offer a more precise view of the cascade of Upf1-dependent events leading to PTC-containing mRNA decay (Fig. 6). The delayed process of release factors recruitment and ribosome recycling upon premature translation termination, favor the recruitment of Upf1 to the terminating ribosome [80–82]. This contact is facilitated by the promiscuous Upf1 binding to RNA enriched onto mRNA 3′UTR [2, 83–85]. This step coincides with Upf1-dependent recruitment of the Upf2/Upf3 heterodimer [45, 86] that also contributes to delay translation termination [87]. In the Upf1-2/3 complex, Upf1 would no longer be strongly bound to RNA [67, 79]. Next, a molecular switch that remains to be characterized displaces Upf2/3 thus allowing assembly of the Upf1-decapping complex [45]. Contact with the nearby RNA and assembly of the decapping complex may contribute to detaching Upf2 from Upf1, as Upf1's interaction with Upf2 is incompatible with RNA and Dcp2 binding (Fig. 5). In the Upf1-decapping complex, Upf1 stably bound to RNA in the presence of its cofactors, anchors the major decay factors Dcp1–Dcp2 establishing the irreversible step toward RNA degradation.

The *in vitro* approaches employed in this study allowed zooming in on important molecular interactions between Upf1, its NMD partners, the decay machinery and the RNA. These insights pave the way for more extensive structural studies and improve our understanding of conserved NMD mechanisms in eukaryotes. However, this experimental strategy faces several limitations such as the difficulty to produce high yields of full-length isoforms for each protein and thus to include all NMD factors, such as Upf3. So, if our strategy allows describing important interactions, we cannot exclude complementary or alternative interactions between NMD factors. Although we expressed multiple recombinant protein isoforms, we may have missed additional contacts offered by full-length and post-translationally modified proteins. Other factors that we did not include in our reconstitution may have important roles, such as the decapping cofactor Edc3, which facilitates the association of Upf1 with Dcp2 *in vivo* and activates Dcp2 [45, 47, 48, 88], or the protein kinase Hrr25, which likely transiently interacts with Upf1 and may participate in post-translational modifications [45]. Moreover, NMD is a highly dynamic process and transitions between successive complexes from translation termination and RNA decay as well as the modulation of enzymatic activities are challenging to catch *in vitro*. For example, identifying the molecular determinant that controls the switch between the Upf1-2/3 detector complex and the Upf1-decapping complex will be key to understanding the NMD pathway.

Acknowledgements

We thank Z. Fourati and B. Seraphin for plasmids; F. Bonneau, G. Badis-Breard, F. Fiorini, and members of our laboratory for insightful discussions; O. Bensaude and B. Seraphin for manuscript proofreading and correction; Ecole doctorale Complexité du Vivant (ED 515, Sorbonne Université) and Agence pour la Recherche contre le Cancer for PhD funding of N.R.-G.; Agence Nationale de la Recherche (ANR-18-CE11-0003; ANR-18-CE11-0003-04; ANR-22-CE12-0004-02) for funding the project; Ecole doctorale IP Paris (ED 626, In-

stitut Polytechnique de Paris) and Fondation ARC pour la Recherche sur le Cancer for PhD funding of I.B.-B.

Author contributions: H.L.H, C.S., and M.G. conceived the project. N.R.-G., H.L.H., and M.G. designed the experiments. N.R.-G. cloned and purified most proteins and performed *in vitro* pulldowns with the help of J.D., E.A., and H.L.H. I.B.-B. cloned and purified Upf2-Ct and HisZZ-Nmd4. C.G.-P. cloned GST-Dcp1/Dcp2-L2. M.G. performed and analyzed AlphaFold3 simulations, sequence alignments, and fluorescence anisotropy assays. H.L.H. performed EMSA assays. N.R.-G., M.G., and H.L.H. analyzed the data. N.R.-G., H.L.H., and M.G. wrote the paper with the input of all other authors.

Supplementary data

Supplementary data is available at NAR online.

Conflict of interest

The authors declare no competing financial interests.

Funding

Ecole doctorale Complexité du Vivant (ED 515, Sorbonne Université) and Agence pour la Recherche contre le Cancer for PhD funding of N.R.-G.; Agence Nationale de la Recherche (ANR-18-CE11-0003; ANR-18-CE11-0003-04; ANR-22-CE12-0004-02) for funding the project; Ecole doctorale IP Paris (ED 626, Institut Polytechnique de Paris) and Fondation ARC pour la Recherche sur le Cancer for PhD funding of I.B.-B. Funding to pay the Open Access publication charges for this article was provided by the CNRS.

Data availability

All data generated or analyzed during this study are included in this published article and its Supplementary Data files. Plasmids generated used in this study are available from the corresponding author upon reasonable request.

References

1. Malabat C, Feuerbach F, Ma L *et al.* Quality control of transcription start site selection by nonsense-mediated-mRNA decay. *eLife* 2015;**4**:e06722. https://doi.org/10.7554/eLife.06722
2. Johansson MJO, He F, Spatrick P *et al.* Association of yeast Upf1p with direct substrates of the NMD pathway. *Proc Natl Acad Sci USA* 2007;**104**:20872–7. https://doi.org/10.1073/pnas.0709257105
3. Brogna S, McLeod T, Petric M. The meaning of NMD: translate or perish. *Trends Genet* 2016;**32**:395–407. https://doi.org/10.1016/j.tig.2016.04.007
4. Celik A, Baker R, He F *et al.* High-resolution profiling of NMD targets in yeast reveals translational fidelity as a basis for substrate selection. *RNA* 2017;**23**:735–48. https://doi.org/10.1261/rna.060541.116
5. Li T, Shi Y, Wang P *et al.* Smg6/Est1 licenses embryonic stem cell differentiation via nonsense-mediated mRNA decay. *EMBO J* 2015;**34**:1630–47. https://doi.org/10.15252/embj.201489947
6. Huth M, Santini L, Galimberti E *et al.* NMD is required for timely cell fate transitions by fine-tuning gene expression and regulating translation. *Genes Dev* 2022;**36**:348–67. https://doi.org/10.1101/gad.347690.120
7. Karam R, Lou C-H, Kroeger H *et al.* The unfolded protein response is shaped by the NMD pathway. *EMBO Rep* 2015;**16**:599–609. https://doi.org/10.15252/embr.201439696
8. Li S, Wilkinson MF. Nonsense surveillance in lymphocytes? *Immunity* 1998;**8**:135–41. https://doi.org/10.1016/S1074-7613(00)80466-5
9. Gloggnitzer J, Akimcheva S, Srinivasan A *et al.* Nonsense-mediated mRNA decay modulates immune receptor levels to regulate plant antibacterial defense. *Cell Host Microbe* 2014;**16**:376–90. https://doi.org/10.1016/j.chom.2014.08.010
10. Lindeboom RGH, Supek F, Lehner B. The rules and impact of nonsense-mediated mRNA decay in human cancers. *Nat Genet* 2016;**48**:1112–8. https://doi.org/10.1038/ng.3664
11. Jaffrey SR, Wilkinson MF. Nonsense-mediated RNA decay in the brain: emerging modulator of neural development and disease. *Nat Rev Neurosci* 2018;**19**:715–28. https://doi.org/10.1038/s41583-018-0079-z
12. Nasif S, Contu L, Mühlemann O. Beyond quality control: the role of nonsense-mediated mRNA decay (NMD) in regulating gene expression. *Semin Cell Dev Biol* 2018;**75**:78–87. https://doi.org/10.1016/j.semcdb.2017.08.053
13. Applequist SE, Selg M, Raman C *et al.* Cloning and characterization of HUPF1, a human homolog of the *Saccharomyces cerevisiae* nonsense mRNA-reducing UPF1 protein. *Nucleic Acids Res* 1997;**25**:814–21. https://doi.org/10.1093/nar/25.4.814
14. Serin G, Gersappe A, Black JD *et al.* Identification and characterization of human orthologues to *Saccharomyces cerevisiae* Upf2 protein and Upf3 protein (*Caenorhabditis elegans* SMG-4). *Mol Cell Biol* 2001;**21**:209–23. https://doi.org/10.1128/MCB.21.1.209-223.2001
15. Bhattacharya A, Czaplinski K, Trifillis P *et al.* Characterization of the biochemical properties of the human Upf1 gene product that is involved in nonsense-mediated mRNA decay. *RNA* 2000;**6**:1226–35. https://doi.org/10.1017/S1355838200000546
16. Chakrabarti S, Jayachandran U, Bonneau F *et al.* Molecular mechanisms for the RNA-dependent ATPase activity of Upf1 and its regulation by Upf2. *Mol Cell* 2011;**41**:693–703. https://doi.org/10.1016/j.molcel.2011.02.010
17. Kanaan J, Raj S, Decourty L *et al.* UPF1-like helicase grip on nucleic acids dictates processivity. *Nat Commun* 2018;**9**:3752. https://doi.org/10.1038/s41467-018-06313-y
18. Fiorini F, Bagchi D, Hir HL *et al.* Human Upf1 is a highly processive RNA helicase and translocase with RNP remodelling activities. *Nat Commun* 2015;**6**:7581. https://doi.org/10.1038/ncomms8581
19. Weng Y, Czaplinski K, Peltz SW. Genetic and biochemical characterization of mutations in the ATPase and helicase regions of the Upf1 protein. *Mol Cell Biol* 1996;**16**:5477–90. https://doi.org/10.1128/MCB.16.10.5477
20. He F, Brown AH, Jacobson A. Upf1p, Nmd2p, and Upf3p are interacting components of the yeast nonsense-mediated mRNA decay pathway. *Mol Cell Biol* 1997;**17**:1580–94. https://doi.org/10.1128/MCB.17.3.1580
21. Lykke-Andersen J, Shu MD, Steitz JA. Human Upf proteins target an mRNA for nonsense-mediated decay when bound downstream of a termination codon. *Cell* 2000;**103**:1121–31. https://doi.org/10.1016/S0092-8674(00)00214-2
22. Amrani N, Ganesan R, Kervestin S *et al.* A faux 3′-UTR promotes aberrant termination and triggers nonsense-mediated mRNA decay. *Nature* 2004;**432**:112–8. https://doi.org/10.1038/nature03060
23. Ivanov PV, Gehring NH, Kunz JB *et al.* Interactions between UPF1, eRFs, PABP and the exon junction complex suggest an integrated model for mammalian NMD pathways. *EMBO J* 2008;**27**:736–47. https://doi.org/10.1038/emboj.2008.17
24. Wu C, Roy B, He F *et al.* Poly (A)-binding protein regulates the efficiency of translation termination. *Cell Rep* 2020;**33**:108399. https://doi.org/10.1016/j.celrep.2020.108399

25. Kurosaki T, Maquat LE. Nonsense-mediated mRNA decay in humans at a glance. *J Cell Sci* 2016;**129**:461–7. https://doi.org/10.1242/jcs.181008
26. Yamashita A, Ohnishi T, Kashima I *et al.* Human SMG-1, a novel phosphatidylinositol 3-kinase-related protein kinase, associates with components of the mRNA surveillance complex and is involved in the regulation of nonsense-mediated mRNA decay. *Genes Dev* 2001;**15**:2215–28. https://doi.org/10.1101/gad.913001
27. Grimson A, O'Connor S, Newman CL *et al.* SMG-1 is a phosphatidylinositol kinase-related protein kinase required for nonsense-mediated mRNA decay in *Caenorhabditis elegans*. *Mol Cell Biol* 2004;**24**:7483–90. https://doi.org/10.1128/MCB.24.17.7483-7490.2004
28. Ohnishi T, Yamashita A, Kashima I *et al.* Phosphorylation of hUPF1 induces formation of mRNA surveillance complexes containing hSMG-5 and hSMG-7. *Mol Cell* 2003;**12**:1187–200. https://doi.org/10.1016/S1097-2765(03)00443-X
29. Chakrabarti S, Bonneau F, Schüssler S *et al.* Phospho-dependent and phospho-independent interactions of the helicase UPF1 with the NMD factors SMG5-SMG7 and SMG6. *Nucleic Acids Res* 2014;**42**:9447–60. https://doi.org/10.1093/nar/gku578
30. Boehm V, Kueckelmann S, Gerbracht JV *et al.* SMG5-SMG7 authorize nonsense-mediated mRNA decay by enabling SMG6 endonucleolytic activity. *Nat Commun* 2021;**12**:3965. https://doi.org/10.1038/s41467-021-24046-3
31. Nagy E, Maquat LE. A rule for termination-codon position within intron-containing genes: when nonsense affects RNA abundance. *Trends Biochem Sci* 1998;**23**:198–9. https://doi.org/10.1016/S0968-0004(98)01208-0
32. Thermann R, Neu-Yilik G, Deters A *et al.* Binary specification of nonsense codons by splicing and cytoplasmic translation. *EMBO J* 1998;**17**:3484–94. https://doi.org/10.1093/emboj/17.12.3484
33. Zhang J, Sun X, Qian Y *et al.* Intron function in the nonsense-mediated decay of β-globin mRNA: indications that pre-mRNA splicing in the nucleus can influence mRNA translation in the cytoplasm. *RNA* 1998;**4**:801–15. https://doi.org/10.1017/S1355838298971849
34. Cho H, Kim KM, Kim YK. Human proline-rich nuclear receptor coregulatory protein 2 mediates an interaction between mRNA surveillance machinery and decapping complex. *Mol Cell* 2009;**33**:75–86. https://doi.org/10.1016/j.molcel.2008.11.022
35. Cho H, Han S, Choe J *et al.* SMG5–PNRC2 is functionally dominant compared with SMG5–SMG7 in mammalian nonsense-mediated mRNA decay. *Nucleic Acids Res* 2013;**41**:1319–28. https://doi.org/10.1093/nar/gks1222
36. Eberle AB, Lykke-Andersen S, Mühlemann O *et al.* SMG6 promotes endonucleolytic cleavage of nonsense mRNA in human cells. *Nat Struct Mol Biol* 2009;**16**:49–55. https://doi.org/10.1038/nsmb.1530
37. Huntzinger E, Kashima I, Fauser M *et al.* SMG6 is the catalytic endonuclease that cleaves mRNAs containing nonsense codons in metazoan. *RNA* 2008;**14**:2609–17. https://doi.org/10.1261/rna.1386208
38. Gatfield D, Izaurralde E. Nonsense-mediated messenger RNA decay is initiated by endonucleolytic cleavage in Drosophila. *Nature* 2004;**429**:575–8. https://doi.org/10.1038/nature02559
39. Unterholzner L, Izaurralde E. SMG7 acts as a molecular link between mRNA surveillance and mRNA decay. *Mol Cell* 2004;**16**:587–96. https://doi.org/10.1016/j.molcel.2004.10.013
40. Loh B, Jonas S, Izaurralde E. The SMG5-SMG7 heterodimer directly recruits the CCR4-NOT deadenylase complex to mRNAs containing nonsense codons via interaction with POP2. *Genes Dev* 2013;**27**:2125–38. https://doi.org/10.1101/gad.226951.113
41. Muhlrad D, Parker R. Premature translational termination triggers mRNA decapping. *Nature* 1994;**370**:578–81. https://doi.org/10.1038/370578a0
42. Charenton C, Graille M. mRNA decapping: finding the right structures. *Phil Trans R Soc B* 2018;**373**:20180164. https://doi.org/10.1098/rstb.2018.0164
43. He F, Jacobson A. Eukaryotic mRNA decapping factors: molecular mechanisms and activity. *FEBS J* 2023;**290**:5057–85. https://doi.org/10.1111/febs.16626
44. Dijk E, Cougot N, Meyer S *et al.* Human Dcp2: a catalytically active mRNA decapping enzyme located in specific cytoplasmic structures. *EMBO J* 2002;**21**:6915–24. https://doi.org/10.1093/emboj/cdf678
45. Dehecq M, Decourty L, Namane A *et al.* Nonsense-mediated mRNA decay involves two distinct Upf1-bound complexes. *EMBO J* 2018;**37**:e99278. https://doi.org/10.15252/embj.201899278
46. He F, Jacobson A. Identification of a novel component of the nonsense-mediated mRNA decay pathway by use of an interacting protein screen. *Genes Dev* 1995;**9**:437–54. https://doi.org/10.1101/gad.9.4.437
47. He F, Wu C, Jacobson A. Dcp2 C-terminal *cis*-binding elements control selective targeting of the decapping enzyme by forming distinct decapping complexes. *eLife* 2022;**11**:e74410. https://doi.org/10.7554/eLife.74410
48. Charenton C, Taverniti V, Gaudon-Plesse C *et al.* Structure of the active form of Dcp1–Dcp2 decapping enzyme bound to m^7GDP and its Edc3 activator. *Nat Struct Mol Biol* 2016;**23**:982–6. https://doi.org/10.1038/nsmb.3300
49. Barbarin-Bocahu I, Ulryck N, Rigobert A *et al.* Identification of an evolutionary conserved binding motif responsible for the recruitment of NMD factors to the UPF1 helicase.*PLoS Biol* 2024;**22**:e3002821. https://doi.org/10.1101/2024.02.27.582253
50. Busetto V, Barbosa I, Basquin J *et al.* Structural and functional insights into CWC27/CWC22 heterodimer linking the exon junction complex to spliceosomes. *Nucleic Acids Res* 2020;**48**:5670–83. https://doi.org/10.1093/nar/gkaa267
51. Fiorini F, Bonneau F, Le Hir H. Biochemical characterization of the RNA helicase UPF1 involved in nonsense-mediated mRNA decay. In: Jankowsky E (ed.), *Methods in Enzymology, RNA Helicases*. Vol. **511**, Elsevier, 2012, 255–74.
52. Ruiz-Gutierrez N, Rieu M, Ouellet J *et al.* Novel approaches to study helicases using magnetic tweezers. *Methods Enzymol* 2022;**673**:359-403. https://doi.org/10.1016/bs.mie.2022.03.035
53. Abramson J, Adler J, Dunger J *et al.* Accurate structure prediction of biomolecular interactions with AlphaFold 3. *Nature* 2024;**630**:493–500. https://doi.org/10.1038/s41586-024-07487-w
54. Jumper J, Evans R, Pritzel A *et al.* Highly accurate protein structure prediction with AlphaFold. *Nature* 2021;**596**:583–9. https://doi.org/10.1038/s41586-021-03819-2
55. Altschul SF, Madden TL, Schäffer AA *et al.* Gapped BLAST and PSI-BLAST: a new generation of protein database search programs. *Nucleic Acids Res* 1997;**25**:3389–402. https://doi.org/10.1093/nar/25.17.3389
56. He F, Jacobson A. Control of mRNA decapping by positive and negative regulatory elements in the Dcp2 C-terminal domain. *RNA* 2015;**21**:1633–47. https://doi.org/10.1261/rna.052449.115
57. Fiorini F, Boudvillain M, Le Hir H. Tight intramolecular regulation of the human Upf1 helicase by its N- and C-terminal domains. *Nucleic Acids Res* 2013;**41**:2404–15. https://doi.org/10.1093/nar/gks1320
58. She M, Decker CJ, Svergun DI *et al.* Structural basis of dcp2 recognition and activation by dcp1. *Mol Cell* 2008;**29**:337–49. https://doi.org/10.1016/j.molcel.2008.01.002
59. Harigaya Y, Jones BN, Muhlrad D *et al.* Identification and analysis of the interaction between Edc3 and Dcp2 in *Saccharomyces cerevisiae*. *Mol Cell Biol* 2010;**30**:1446–56. https://doi.org/10.1128/MCB.01305-09
60. Charenton C, Gaudon-Plesse C, Fourati Z *et al.* A unique surface on Pat1 C-terminal domain directly interacts with Dcp2 decapping enzyme and Xrn1 5′-3′ mRNA exonuclease in yeast. *Proc Natl Acad Sci USA* 2017;**114**:E9493–501. https://doi.org/10.1073/pnas.1711680114
61. Barbarin-Bocahu I, Graille M. The X-ray crystallography phase problem solved thanks to AlphaFold and RoseTTAFold models: a

case-study report. *Acta Crystallogr Sect Struct Biol* 2022;**78**:517–31. https://doi.org/10.1107/S2059798322002157
62. Luke B, Azzalin CM, Hug N *et al.* Saccharomyces cerevisiae Ebs1p is a putative ortholog of human Smg7 and promotes nonsense-mediated mRNA decay. *Nucleic Acids Res* 2007;**35**:7688–97. https://doi.org/10.1093/nar/gkm912
63. Chen H, Xue J, Churikov D *et al.* Structural insights into yeast telomerase recruitment to telomeres. *Cell* 2018;**172**:331–43. https://doi.org/10.1016/j.cell.2017.12.008
64. Varadi M, Bertoni D, Magana P *et al.* AlphaFold Protein Structure Database in 2024: providing structure coverage for over 214 million protein sequences. *Nucleic Acids Res* 2024;**52**:D368–75. https://doi.org/10.1093/nar/gkad1011
65. Jonas S, Weichenrieder O, Izaurralde E. An unusual arrangement of two 14-3-3-like domains in the SMG5–SMG7 heterodimer is required for efficient nonsense-mediated mRNA decay. *Genes Dev* 2013;**27**:211–25. https://doi.org/10.1101/gad.206672.112
66. Uetz P, Giot L, Cagney G *et al.* A comprehensive analysis of protein–protein interactions in Saccharomyces cerevisiae. *Nature* 2000;**403**:623–7. https://doi.org/10.1038/35001009
67. Chamieh H, Ballut L, Bonneau F *et al.* NMD factors UPF2 and UPF3 bridge UPF1 to the exon junction complex and stimulate its RNA helicase activity. *Nat Struct Mol Biol* 2008;**15**:85–93. https://doi.org/10.1038/nsmb1330
68. Kadlec J, Izaurralde E, Cusack S. The structural basis for the interaction between nonsense-mediated mRNA decay factors UPF2 and UPF3. *Nat Struct Mol Biol* 2004;**11**:330–7. https://doi.org/10.1038/nsmb741
69. Fourati Z, Roy B, Millan C *et al.* A highly conserved region essential for NMD in the Upf2 N-terminal domain. *J Mol Biol* 2014;**426**:3689–702. https://doi.org/10.1016/j.jmb.2014.09.015
70. Melero R, Uchiyama A, Castaño R *et al.* Structures of SMG1-UPFs complexes: SMG1 contributes to regulate UPF2-dependent activation of UPF1 in NMD. *Struct Lond Engl 1993* 2014;**22**:1105–19.
71. Clerici M, Mourão A, Gutsche I *et al.* Unusual bipartite mode of interaction between the nonsense-mediated decay factors, UPF1 and UPF2. *EMBO J* 2009;**28**:2293–306. https://doi.org/10.1038/emboj.2009.175
72. Cheng Z, Muhlrad D, Lim MK *et al.* Structural and functional insights into the human Upf1 helicase core. *EMBO J* 2007;**26**:253–64. https://doi.org/10.1038/sj.emboj.7601464
73. Hug N, Longman D, Cáceres JF. Mechanism and regulation of the nonsense-mediated decay pathway. *Nucleic Acids Res* 2016;**44**:1483–95. https://doi.org/10.1093/nar/gkw010
74. Kurosaki T, Popp MW, Maquat LE. Quality and quantity control of gene expression by nonsense-mediated mRNA decay. *Nat Rev Mol Cell Biol* 2019;**20**:406–20. https://doi.org/10.1038/s41580-019-0126-2
75. Lavysh D, Neu-Yilik G. UPF1-mediated RNA decay—danse macabre in a cloud. *Biomolecules* 2020;**10**::999. https://doi.org/10.3390/biom10070999
76. Kadlec J, Guilligay D, Ravelli RB *et al.* Crystal structure of the UPF2-interacting domain of nonsense-mediated mRNA decay factor UPF1. *RNA* 2006;**12**:1817–24. https://doi.org/10.1261/rna.177606
77. Glavan F, Behm-Ansmant I, Izaurralde E *et al.* Structures of the PIN domains of SMG6 and SMG5 reveal a nuclease within the mRNA surveillance complex. *EMBO J* 2006;**25**:5117–25. https://doi.org/10.1038/sj.emboj.7601377
78. Langer LM, Kurscheidt K, Basquin J *et al.* UPF1 helicase orchestrates mutually exclusive interactions with the SMG6 endonuclease and UPF2. *Nucleic Acids Res* 2024;**52**:6036–48. https://doi.org/10.1093/nar/gkae323
79. Xue G, Maciej VD, Machado de Amorim A *et al.* Modulation of RNA-binding properties of the RNA helicase UPF1 by its activator UPF2. *RNA* 2023;**29**:178–87. https://doi.org/10.1261/rna.079188.122
80. Ganesan R, Mangkalaphiban K, Baker RE *et al.* Ribosome-bound Upf1 forms distinct 80S complexes and conducts mRNA surveillance. *RNA* 2022;**28**:1621–42.
81. Schuller AP, Zinshteyn B, Enam SU *et al.* Directed hydroxyl radical probing reveals Upf1 binding to the 80S ribosomal E site rRNA at the L1 stalk. *Nucleic Acids Res* 2018;**46**:2060–73. https://doi.org/10.1093/nar/gkx1263
82. Min EE, Roy B, Amrani N *et al.* Yeast Upf1 CH domain interacts with Rps26 of the 40S ribosomal subunit. *RNA* 2013;**19**:1105–15. https://doi.org/10.1261/rna.039396.113
83. Hogg JR, Goff SP. Upf1 senses 3′UTR length to potentiate mRNA decay. *Cell* 2010;**143**:379–89. https://doi.org/10.1016/j.cell.2010.10.005
84. Hurt JA, Robertson AD, Burge CB. Global analyses of UPF1 binding and function reveal expanded scope of nonsense-mediated mRNA decay. *Genome Res* 2013;**23**:1636–50. https://doi.org/10.1101/gr.157354.113
85. Zünd D, Gruber AR, Zavolan M *et al.* Translation-dependent displacement of UPF1 from coding sequences causes its enrichment in 3′ UTRs. *Nat Struct Mol Biol* 2013;**20**:936–43. https://doi.org/10.1038/nsmb.2635
86. Atkin AL, Schenkman LR, Eastham M *et al.* Relationship between yeast polyribosomes and upf proteins required for nonsense mRNA decay*. *J Biol Chem* 1997;**272**:22163–72. https://doi.org/10.1074/jbc.272.35.22163
87. Neu-Yilik G, Raimondeau E, Eliseev B *et al.* Dual function of UPF3B in early and late translation termination. *EMBO J* 2017;**36**:2968–86. https://doi.org/10.15252/embj.201797079
88. Nissan T, Rajyaguru P, She M *et al.* Decapping activators in Saccharomyces cerevisiae act by multiple mechanisms. *Mol Cell* 2010;**39**:773–83. https://doi.org/10.1016/j.molcel.2010.08.025
89. Gouy M, Guindon S, Gascuel O SeaView Version 4: a multiplatform graphical user interface for sequence alignment and phylogenetic tree building. *Mol Biol Evol* 2010;**27**:221–4. https://doi.org/10.1093/molbev/msp259

Received: October 29, 2024. **Revised:** February 6, 2025. **Editorial Decision:** February 14, 2025. **Accepted:** February 18, 2025